

Characterizing Concentrations and Size Distributions of Metal-Containing Nanoparticles in Waste Water

APM 272

Characterizing Concentrations and Size Distributions of Metal-Containing Nanoparticles in Waste Water

APM 272

Edward M. Heithmar^a
Spiros A. Pergantis^b

^aU.S. Environmental Protection Agency
National Exposure Research Laboratory
Environmental Sciences Division
944 E. Harmon Ave.
Las Vegas, NV 89119

^bNRC Senior Research Fellow
U.S. Environmental Protection Agency
National Exposure Research Laboratory
Environmental Sciences Division
944 E. Harmon Ave.
Las Vegas, NV 89119

Although this work was reviewed by EPA and approved for publication, it may not necessarily reflect official Agency policy. Mention of trade names and commercial products does not constitute endorsement or recommendation for use.

Abstract

Nanomaterials containing metals are finding increasing use in consumer, industrial, and medical products, and they are subsequently being released into the environment. Methods for detecting, quantifying, and characterizing these materials in complex matrices are critical for the eventual understanding of their implications to environmental quality and human health. This report describes recent progress in the development of new metrology tools. Single particle – inductively coupled plasma mass spectrometry (SP-ICPMS) is used to analyze complex aqueous samples. SP-ICPMS simultaneously quantifies the concentration of nanoparticles containing an analyte metal and measures the metal mass in individual nanoparticles. The accuracy of SP-ICPMS is assessed over a range of nanoparticle sizes. The utility of the technique in a number of applications is examined. Nanoparticles containing the analyte element can be measured accurately and precisely in the presence of a 10,000-fold greater concentration of other nanoparticles. SP-ICPMS is used to assess transformation of nanoparticles induced by changes in ionic strength. A screening-level assessment of metal-containing nanoparticles in urban run-off using SP-ICPMS is demonstrated, and preliminary studies of coupling SP-ICPMS with on-line nanoparticle size separation methods are presented.

Notice

The United States Environmental Protection Agency's (EPA) Office of Research and Development performed and funded the research described here. Mention of trade names or commercial products does not constitute endorsement or recommendation for use.

Table of Contents

Abstract	ii
Notice	iii
Table of Contents	iv
Abbreviations and symbols	v
Acknowledgments	vi
Introduction	1
Uses of engineered nanomaterials.	1
Environmental implications of increased use of engineered nanomaterials	2
Rationale for the development of metrology tools for metal-containing ENMs	3
Methods for characterizing engineered nanomaterials	4
Theory of SP-ICPMS	7
Experimental	9
Materials	9
Instrumentation	9
Methods	9
Results and Discussion	10
Assessment of SP-ICPMS accuracy	10
Precision and selectivity of SP-ICPMS	11
Nanoparticle transformation study	11
Screening urban runoff using SP-ICPMS	12
Coupling SP-ICPMS with separation methods	13
Conclusions and Future Work	14
References	16
Tables	22
Figure Captions	26

Abbreviations and symbols

AFM	Atomic force microscopy
c_a	Analyte concentration in aqueous sample (g mL^{-1})
CAPS	3-(cyclohexylamino)propanesulfonic acid
CDF	Cumulative distribution function
CE	Capillary electrophoresis
c_p	Particle concentration in aqueous sample (mL^{-1})
DLS	Dynamic light scattering
EDS	Energy dispersive X-ray spectrometry
EHS	Environmental health and safety
ϵ_n	Nebulization transport efficiency (dimensionless)
ENM	Engineered nanomaterials
EPA	Environmental Protection Agency
ESD	Environmental Sciences Division
FFF	Field flow fractionation
Flow-FFF	Flow field flow fractionation
HDC	Hydrodynamic chromatography
ICPMS	Inductively coupled plasma mass spectrometry
IRZ	Initial radiation zone
$m_{a,p}$	Analyte element mass in the particle (g)
NAZ	Normal analytical zone
$n_{i,p}$	Number of analyte ions detected (unitless number)
NOM	Natural organic matter
NTA	Nanoparticle tracking analysis
$q_{i,a}$	Ionized analyte flux (s^{-1})
q_p	Particle flux (s^{-1})
q_s	Sample uptake rate (mL s^{-1})
r_g	Radius of gyration
r_h	Hydrodynamic radius
SDS	Sodium dodecyl sulfate
Sed-FFF	Sedimentation field flow fractionation
SEM	Scanning electron microscopy
SLS	Static light scattering
SP-ICPMS	Single particle - inductively coupled plasma mass spectrometry
t_d	Dwell time (s)
TEM	Transmission electron microscopy
τ_p	Plume pulse transit time (s)

Acknowledgments

I am grateful to PerkinElmer for providing the DRCE inductively coupled plasma mass spectrometer used for some of this research. Charlita Rosal of EPA developed and performed the capillary electrophoresis separation shown in this report.

Introduction

The National Nanotechnology Initiative defines nanotechnology as “the understanding and control of matter at dimensions between approximately 1 and 100 nanometers”(Council 2010), and nanomaterials are defined as materials with at least one characteristic dimension in this range. Nanomaterials can be natural (e.g., humic and fulvic acids) (Thurman and Malcolm 1981), incidental to human activity (e.g., diesel emissions, welding fumes) (Peters, Elzey et al. 2009), or engineered. Engineered nanomaterials (ENMs) exhibit optical, electrical, and chemical characteristics different from either their bulk or dissolved forms. Because of this, they are the source of the so called nanotechnology revolution. Most ENMs can be divided into two general classes, depending on whether they are carbon-based (e.g., carbon nanotubes and fullerenes) or metal-containing (e.g., Ag, TiO₂, CeO₂, Fe).

Uses of engineered nanomaterials.

The use of ENMs in consumer, industrial, and agricultural products, as well as in environmental technology is rapidly increasing (Ponder, Darab et al. 2001; Chaudhry, Scotter et al. 2008; Nanotechnologies 2010). This is largely due to the unique optical, electrical, and chemical properties of nano-scale particles. Often, the benefit of using nanomaterials stems from the increased surface area per unit mass of material, which increases with the inverse of the diameter in the case of spherical particles. This results in faster rates of chemical reactions such as oxidative catalysis that occur at surfaces. Sometimes the benefit of nanomaterials arises from the quantum nature of energy states at the nanometer scale, as in the wavelength tuning of the fluorescence of quantum dots (Michalet, Pinaud et al. 2005). In the health sciences, the ability of ENMs to bind to cell walls can be utilized for drug delivery (Lai, Trewyn et al. 2003; Zhang, Pornpattananankul et al. 2010).

The Project on Emerging Nanotechnologies maintains a database of consumer products that manufacturers claim contain ENMs (Nanotechnologies 2010). Currently the database contains over 1000 products. Consumer products containing nano-scale silver dominate current ENM usage (Table 1). Note that of the carbon-based ENMs, nearly $\frac{3}{4}$ of the products are durable goods that incorporate carbon nanotubes in the construction material. The nanotubes are bound in this matrix for the lifetime of the product. Conversely, the metal-containing ENMs are most often used in dispersive applications, where they are intentionally released from the product or where incidental release is substantial. For example, fabrics containing nano-scale silver release silver during washing at varying rates, depending on the type of fabric and the washing conditions (Benn and Westerhoff 2008; Geranio, Heuberger et al. 2009). Of the products using carbon-based ENMs only 7 very low-volume uses of fullerenes are documented. Although there is only one product listed using cerium oxide, it is as a diesel fuel additive that potentially could entail high-volume dispersive use.

Environmental implications of increased use of engineered nanomaterials

The unusual properties that result in unique benefits from the use of ENMs have also elicited intense interest in the environmental behavior of these materials. The environmental transport, transformation, fate, exposure potential, and effects of ENMs cannot be predicted by the behavior of either the corresponding dissolved or neat chemicals. In addition, the metrics that affect all these environmental properties are different and more complex than those of conventional pollutants. The number of funded research projects on the environmental health and safety (EHS) implications of ENMs (Figure 1) increased dramatically from 1998 to 2007 (Nanotechnologies 2010). There has been some decline in newly initiated projects in the past two years (although data for 2010 are incomplete); nonetheless, research into EHS of ENMs remains intense. The level of research activity is roughly evenly apportioned to carbon-based and metal containing ENMs. For the former, there are currently about 54 investigations of nanotubes and 29 of fullerenes. Of the metal-containing ENMs, most investigations involve titanium dioxide and iron, followed by quantum dots, silver, and then the remaining metal oxides. The interest in carbon nanotubes stems from the known toxicity of these materials that is mediated by the particle aspect ratio. Research focus on the metal-containing ENMs is prompted by their high likelihood to be released from products. This leads to a greater potential loading of the metal-containing ENMs in environmental compartments.

An essential capability for any successful research into the environmental behavior of ENMs is a set of metrology tools for the several metrics of the materials that control their release transport, transformation, fate, and effects. These tools would also be required for determining the occurrence and distribution of ENMs in the environment, and they would permit the temporal trends in these to be assessed. A previous report by the Environmental Sciences Division (ESD) described the importance of characterization of metal-containing ENMs in the exposure research of these potential environmental stressors (Heithmar 2009). It discussed the several methods currently available for the characterization of various exposure metrics and why the current methods are inadequate. The report introduced single particle – inductively coupled plasma mass spectrometry (SP-ICPMS) as a method for both screening-level and selective determination of metal-containing ENM dispersions. The potential of SP-ICPMS to become the first practical analytical method for characterization of metal-containing ENMs in environmental matrices was demonstrated.

This report describes recent progress in the development of SP-ICPMS, which can simultaneously quantify the concentration of nanoparticles containing an analyte metal and measure the metal mass in individual nanoparticles. The report briefly reviews the current metrology methods discussed in the previous report and introduces two not covered there. The introduction concludes with a conceptual description of SP-ICPMS, with a real analytical example, and the equations and associated assumptions to calibrate the method. The experiments discussed in this report first assess the accuracy of SP-ICPMS over a range of nanoparticle sizes. The utility of the technique in a number of applications is then examined.

Nanoparticles containing the analyte element can be measured accurately and precisely in the presence of a 10,000-fold greater concentration of other nanoparticles. SP-ICPMS is used to assess transformation of nanoparticles induced by changes in ionic strength. Limitations in sampling and sample handling of real environmental water samples for nanoparticle measurements are demonstrated. A screening-level assessment of metal-containing nanoparticles in urban run-off using SP-ICPMS is demonstrated. Finally, preliminary studies of coupling SP-ICPMS with on-line nanoparticle size separation methods are presented.

Rationale for the development of metrology tools for metal-containing ENMs

A 2009 workshop of approximately 50 scientists involved in EHS research of ENMs was sponsored by the International Council on Nanotechnology (ICON). The charge of the workshop was to identify and rank the key research priorities for informed decisions on developing ENMs with minimal potential adverse environmental impacts. The workshop report (Alvarez, Colvin et al. 2009) identified fourteen research priorities, which were ranked according to two criteria: (1) the importance of each issue in advancing our ability to design ENMs responsibly, and (2) the current development of scientific understanding of the issue. Tools to detect, measure and characterize ENMs ranked highest in importance. This area was also determined to be the most poorly developed. Consequently, development of metrology tools, especially for real environmental matrices, was the highest ranked research priority.

The first reason for the critical need for research to develop metrology tools is their central role in every area of EHS research. These areas include (1) measuring the environmental occurrence and distribution of ENMs, (2) determining temporal trends in environmental loads, (3) laboratory studies of transport, transformation, and fate, and (3) toxicity studies. Ultimately, exposure models must be developed for ENMs (Mueller and Nowack 2008), and these will require measuring releases for source terms, as well as measuring ENM distributions in the environment to verify the models.

Another reason for developing ENM metrology tools is the complex set of metrics. For conventional pollutants, mass concentration is often the only relevant metric for determining exposure. In the case of ENMs, exposure potential is affected by particle size. Depending on the exposure model, measurement of size distributions in terms of particle mass, volume, or equivalent hydrodynamic radius may be most relevant (Hassellöv, Readman et al. 2008). Specific surface area (area/mass ratio) is important to the catalytic activity of ENMs such as TiO₂, and it can influence toxicity (Schulte, Geraci et al. 2008). Surface charge and the related property of ζ potential can determine the degree ENMs tend to aggregate (Kim, Lee et al. 2008). As previously discussed, particle shape, characterized by aspect ratio, can dramatically affect toxicity of carbon nanotubes (Magrez, Kasas et al. 2006; Takagi, Hirose et al. 2008).

A third factor fueling the high interest in developing ENM metrology tools is the current lack of many practical methods. There are a number of techniques for measuring concentrations and size distributions of ENMs in pure suspensions used as starting materials in laboratory

studies. However, very few methods exist for detection, quantification, and characterization of suspensions after they are introduced into test systems. Such techniques are critical, because the ENM can transform in the test system (Alvarez, Colvin et al. 2009). Going one step further in complexity, virtually no practical methods have been published for measuring concentration and size distributions of ENMs in real environmental samples (Handy, von der Kammer et al. 2008). There are two reasons for this situation. First, concentrations of ENMs in the real environment are very low (Benn and Westerhoff 2008). Compounding this low concentration is the presence of natural colloids that interfere (Klaine, Alvarez et al. 2008), especially in the case of metal-containing ENMs. Detection and quantification of metals usually involves measuring total element concentration, and natural colloids often include minerals that contain the same element as the ENM of interest. In addition, analyte elements can also adsorb on natural organic matter (NOM) in colloids.

Advances in understanding the environmental behavior of metal-containing ENMs can only be made if detection, quantification, and characterization methods are developed, especially for the concentration and size distribution metrics of the nanomaterials. In the short term, these methods must be effective at least in laboratory test systems, and at least screening-level methods must be available to detect the probable presence of metal-containing ENMs in real environmental samples. Ultimately, selective determinative methods that greatly minimize false positives in real-world samples must be developed. The development of characterization methods for metrics other than nanoparticle concentration and size distribution may never be attainable for these systems.

Methods for characterizing engineered nanomaterials

Methods that are currently available to measure several common ENM characterization metrics (Table 2, adapted from Heithmar 2009a) generally work well in simple matrices. One general class of characterization techniques is single particle imaging. The most common of these methods are scanning electron microscopy (SEM) or transmission electron microscopy (TEM) (Lin and Yang 2005; Pyrz and Buttrey 2008). In well controlled systems, atomic force microscopy (AFM) can be advantageous, because interaction forces between ENMs and substrates can be studied (Ebenstein, Nahum et al. 2002). When combined with X-ray emission spectroscopy, usually in the energy dispersive mode (EDS), SEM or TEM can definitively identify ENMs in a simple sample matrix. However, particle concentration must be generally at least 10^9 mL^{-1} with current sampling methods, making the use of this method for environmentally relevant concentrations of ENMs infeasible. Representative sampling of the test material is generally not attainable, so quantification is impossible. In environmental samples, distinguishing metal-containing ENMs from colloids containing the same metal is difficult (Tiede, Hassellöv et al. 2009). Finally, sampling methods can introduce artifacts, especially in the size distribution of ENMs (Tang, Wu et al. 2009).

An alternative to single-particle imaging for characterizing nanoparticle concentration and size distribution is the general class of ensemble measurement techniques, in which a signal produced by a sample population of particles is measured. Several light scattering methods are

among the ensemble approaches, and they can provide representative size distribution characterization at relatively low concentrations (ca. 10^7 - 10^8 mL⁻¹). Dynamic light scattering (DLS), also called photon correlation spectroscopy, measures the decay of the autocorrelation of laser light scattering to calculate the hydrodynamic radius (r_h) distribution (Filella, Zhang et al. 1997). DLS combined with applying an oscillating electric field also can measure ζ potential, which is related to the surface charge of an ENM. Static light scattering (SLS), which measures the continuous scatter signal at various scattering angles, provides the complementary size characteristic of radius of gyration (r_g) (Kammer, Baborowski et al. 2005). The ratio r_g/r_h can provide an estimation of ENM shape (Schurtenberger, Newmen et al. 1993). Unfortunately, both these ensemble laser light scattering methods are prone to errors in widely polydisperse suspensions, because scatter signal is exponentially related to size. Nanoparticle tracking analysis (NTA) is a single particle light scattering technique that does not suffer this limitation. None of the light scattering techniques are effective in complex media with multiple particle types, because they do not measure particle elemental composition.

Field flow fractionation (FFF) has become popular for physical separation of nanoparticles of different sizes. It can be used with an ensemble detector, such as inductively coupled plasma mass spectrometry (ICPMS), that can provide elemental concentration for each size fraction. Therefore, the FFF-ICPMS combination is applicable in complex systems. FFF is actually a general technique with several implementations. All the FFF methods use the application of a laminar flow of eluent through a narrow channel combined with an orthogonal force field (hence the term field flow). In most implementations of FFF, the orthogonal force field results in bigger particles having an average position closer to the channel wall than smaller particles, resulting in a lower average velocity for the bigger particles, and a resulting size separation at the channel outlet. The two commonly used FFF techniques for ENM characterization are flow field (flow-FFF) (Stolpe, Hassellöv et al. 2005; Leshner, Ranville et al. 2009) or, to a lesser extent, a sedimentation (gravity) field (sed-FFF) (Taylor, Garbarino et al. 1992; Hassellöv, Lyvén et al. 1999). Flow-FFF separates nanoparticle sizes by hydrodynamic radius, while sed-FFF separates by buoyant mass. Flow-FFF combined with ICPMS detection has recently been used to study the adsorption of uranium ions on iron oxide nanoparticles (Leshner, Ranville et al. 2009).

Another technique for physically separating nanoparticle size fractions that has recently been applied to ENMs is hydrodynamic chromatography (HDC) (Tiede, Hassellöv et al. 2009). HDC can be coupled on-line with ICPMS to provide an ensemble characterization method (Tiede, Boxall et al. 2010). In HDC, the sample is passed through a column of inert material such as silica with a mobile phase. The inter-particle channels in the stationary phase approach the size of the nanoparticles, so that nanoparticles with larger hydrodynamic radius experience a higher average velocity of the laminar flow of mobile phase than smaller particles. Thus, larger particles elute before smaller ones. HDC potentially has less likelihood for artifacts due to interactions with the stationary phase than FFF methods, which use semi-permeable polymer membranes. On the other hand, FFF provides separations of higher size resolution.

Capillary electrophoresis (CE) has recently been applied to separation of engineered nanomaterials (Liu and Wei 2004; Liu, Lin et al. 2005). CE has the advantage of relatively fast

analysis compare with FFF and HDC, and very good theoretical resolving power. It separates nanoparticles based on electrophoretic mobility (Petersen and Ballou 1992; Huff and McIntire 1994; Quang, Petersen et al. 1996). Therefore, nanoparticle charge and size both affect retention time. This can lead to complications in data interpretation.

Ensemble methods based on size separation coupled on-line with elemental detection (i.e., hyphenated methods) provide elemental information in addition to size distribution. This level of specificity makes them effective tools in moderately complex systems like laboratory test media. However, they can only give screening-level characterization of real environmental samples. They provide the information on total analyte element content associated with different size particles. Therefore, they cannot distinguish a large concentration of nanoparticles, each containing a small fraction of analyte element, from a lower concentration of the same size particles, each with a high analyte element fraction. For example, a large background of natural organic matter of 20 nm hydrodynamic radius with adsorbed silver ions cannot be distinguished from a low concentration of 20 nm silver nanoparticles.

The lack of any practical methods for detecting, quantifying, and characterizing metal-containing ENMs in environmental media has resulted in the adaptation of a single particle technique from aerosol analysis and colloid chemistry. This method, as modified in our laboratory for aqueous suspensions of metal-containing ENMs, is called single particle-inductively coupled plasma mass spectrometry. A related technique was originally developed to characterize airborne particulates (Nomizu, Nakashima et al. 1992; Nomizu, Hayashi et al. 2002). That technique was later adapted for characterizing zirconia colloids (Degueldre, Favarger et al. 2004), thorium oxide (Degueldre and Favarger 2004), and gold particles (Degueldre, Favarger et al. 2006). Recently, the technique was applied to characterize silver nanoparticles in municipal waste water (Monserud, Leshner et al. 2009), and preliminary results of the technique coupled with flow-FFF have been presented (Hassellöv 2009). ESD presented a study of the performance of SP-ICPMS and how ICPMS acquisition and plasma parameters control performance (Heithmar 2009).

SP-ICPMS relies on the fact that metal-containing nanoparticles entering an ICPMS plasma produce intense ion plumes of the metal isotopes in very short time periods (< 1 ms). If the ICPMS signal is monitored very fast (≤ 10 ms data points), any moderate background from dissolved analyte metal, or plasma matrix ions (Lam and Horlick 1990), diminishes to an average count of less than 1 ion detected per data point. The ion plume pulses from the nanoparticles are easily distinguished. The frequency of the pulses is proportional to the nanoparticle concentration in the sample, and the number of ions detected in each pulse is proportional to the analyte mass in the nanoparticle creating the pulse.

SP-ICPMS is a single particle rather than an ensemble method, so it analyzes individual nanoparticles (Table 3). SP-ICPMS does not measure particle size, but rather analyte mass for each particle and the nanoparticle concentration. The hyphenated methods do not give information on individual nanoparticles, but rather on each size fraction of nanoparticles as a group. One other difference between SP-ICPMS and the hyphenated methods is that the former measurement is made on a time scale of several seconds to a minute depending on the

concentration, while the latter typically require 10 – 30 minutes. It can be seen that SP-ICPMS and the hyphenated approaches are complementary, and preliminary results of coupling the two will be discussed in this report.

Theory of SP-ICPMS

A detailed description of ICPMS processes in the conventional mode as well as in the SP mode was given in our previous report (Heithmar 2009). This report gives a conceptual description of the techniques with real analytical results to demonstrate the concepts.

In conventional ICPMS, an aerosol of droplets is produced from the sample usually using some form of pneumatic nebulizer (Taylor 2001). The larger aerosol droplets are removed by collisions within a spray chamber before a tertiary aerosol of droplets enters the plasma. The flux of droplets is typically greater than 10^6 s^{-1} . Each droplet contains a few hundred to a few thousand analyte atoms. The efficiency of the sampling process from aqueous sample to aerosol flux in the plasma is quantified by the nebulization transport efficiency, ϵ_n , which is generally between 2% and 30%, depending on the nebulizer and spray chamber used. The aerosol is evaporated in the preheating zone of the plasma, within the load coil region. The salt residues containing the analyte begin to vaporize in this region. The salts are atomized in the initial radiation zone (IRZ), which extends from the load coil several mm (Koirtyohann, Jones et al. 1980). Ionization occurs in the normal analytical zone (NAZ) (Thomas 2004). The vaporization, atomization, and ionization processes are usually >80% efficient for most elements (O'Connor and Evans 1999).

In conventional ICPMS, the above processes result in a fairly constant flux of analyte ions reaching the detector, due to the large number of droplets and the small number of analyte atoms dissolved in each droplet. The resulting ICPMS signal for 30 pg/mL dissolved gold with a short measurement window (known as the dwell time, t_d) of 10 ms is very low and somewhat noisy (Figure 2a). Therefore, a longer measurement window is usually used in conventional ICPMS (Figure 2b). The signal for the 30 pg/mL dissolved gold is roughly constant at about 80 s^{-1} .

When the same 30 ng of gold in 50 nm nanoparticles are suspended in each mL of sample, very few aerosol droplets contain any gold, and a few contain ca. 4×10^6 gold atoms (one nanoparticle). The resulting signal (Figure 3a) for the conventional long t_d (2 s in this example) is somewhat noisier than for dissolved gold, which is expected by the episodic nature of the gold flux. The average signal intensity is the same as for the same concentration of dissolved gold (Figure 2b). Each gold nanoparticle produces a plume of millions of ions that enter the mass spectrometer interface over a period of less than 500 μs (Gray, Olesik et al. 2009; Heithmar 2009). In SP-ICPMS, this discrete nature of the ion signal is exploited by using very short dwell times. With $t_d = 10 \text{ ms}$, each gold nanoparticle ion plume reaching the detector contains about 30 ions (the rest of the ions entering the interface are lost in the spectrometer), producing a corresponding pulse (Figure 3b). The number of ions detected in each pulse is directly proportional to the gold mass in the corresponding single nanoparticle. The frequency of pulses is proportional to the concentration of nanoparticles in the sample (in this case, ca. $2 \times 10^4 \text{ mL}^{-1}$).

This theory of SP-ICPMS that results in an easily calibrated signal relies on two assumptions. First, every nanoparticle that reaches the plasma is detected. This also depends on a sufficiently long residence time, so the ion plume expands enough to substantially fill the cross section of the central channel of the plasma. If so, equation 1 is valid.

$$(1) \quad q_p / c_p = q_s \varepsilon_n,$$

where q_p = flux of particles detected in plasma (s^{-1}), c_p = concentration of nanoparticles containing the detected metal in the sample (mL^{-1}), q_s = sample uptake rate ($mL s^{-1}$), and ε_n = nebulization efficiency (dimensionless). Note that q_s and ε_n are properties of the ICPMS instrument conditions, and independent of the element. Therefore, equation 1 can be used to calculate their product using any type of nanoparticle suspension of known c_p .

The second assumption of the SP-ICPMS theory is that ICPMS sensitivity is constant for an analyte, irrespective of whether it is dissolved or contained in nanoparticles. Again, this requires that the residence time in the plasma to be sufficiently long. If so, equation 2 is valid.

$$(2) \quad m_{a,p} = [q_s \varepsilon_n c_a / q_{i,a}] n_{i,p} = k n_{i,p},$$

where $m_{a,p}$ = mass of analyte element in a single nanoparticle (g), $n_{i,p}$ = number of ions of analyte element detected in the corresponding plume (number of ions detected in a single SP-ICPMS pulse – see Figure 3 b), c_a = the analyte concentration in a dissolved standard of the analyte ($g mL^{-1}$), $q_{i,a}$ = ion flux measured for the dissolved standard (s^{-1}). For each analyte element, calibration of the element mass in individual particles (calculation of the response factor k) requires only the $q_s \varepsilon_n$ product from Equation 1 and analysis of a known concentration of dissolved analyte element using a conventional ICPMS standard).

Equation 2 provides calibration of nanoparticle element mass. The calibration of nanoparticle concentration is provided by rearrangement of equation 1 for any unknown nanoparticle suspension, once $q_s \varepsilon_n$ has been determined:

$$(3) \quad c_p = q_p / q_s \varepsilon_n.$$

Experimental

Most of the materials, instrumentation and methods used in the present study are found in our previous report (Heithmar 2009). Only those added or modified are described here.

Materials

Sodium dodecyl sulfate (SDS), Triton X-100, and 3-(cyclohexylamino)propanesulfonic acid (CAPS) were obtained from Sigma-Aldrich, St. Louis, MO. Calcium chloride was obtained from EMD Chemicals, Darmstadt, Germany. Syringe filters (0.45 μm and 5.0 μm nylon) were obtained from Sterlitech, Kent, WA. Urban runoff water for SP-ICPMS experiments were obtained from Las Vegas Wash, Las Vegas, NV (36° 6.826' N, 115° 8.741' W, ca. 2 km east of Las Vegas Blvd.).

Instrumentation

ICPMS analyses were performed on both the DRCe (PerkinElmer, Waltham, MA) described previously and on a 7500ce (Agilent, Santa Clara, CA), with an upgraded 7500cx lens system. HDC-SP-ICPMS experiments were conducted with a hydrodynamic chromatography column (5-300 nm size range, Polymer Laboratories, Shropshire, UK) with either an Agilent 1200 HPLC pump or an 100DM syringe pump (ISCO, Lincoln, NE). CE-ICPMS experiments were conducted with a MDQ capillary electrophoresis instrument (Beckman-Coulter, Brea, CA).

Methods

Because of limitations in software, SP-ICPMS measurements on the 7500ce with dwell times less than 10 ms had to be acquired by entering multiple elements, so the total integration time was at least 10 ms.

Silver nanoparticle transformation studies were conducted on either 500 ng/mL ($4.5 \times 10^8 \text{ mL}^{-1}$ particle concentration) or 0.25 ng/mL ($2.2 \times 10^5 \text{ mL}^{-1}$) silver nanoparticle suspensions in water. The samples were spiked to final concentration of 200 mM CaCl_2 . Subsamples were taken at designated times after spiking and diluted to $1 \times 10^4 \text{ mL}^{-1}$ for SP-ICPMS analysis.

Urban runoff water (10 mL) was collected in polypropylene syringes and filtered on-site with 5.0 μm syringe filters. One sample was spiked with gold and silver nanoparticle suspensions prior to filtering. Samples were analyzed by SP-ICPMS within 36 hours, usually within three hours.

HDC separations were conducted using 10 mM SDS buffer optimized for the nanomaterial. Triton X-100 (0.1%) was added in some experiments. Eluent flow was 1.0

mL/min. The column eluent was split 60/40 with a tee and a PEEK capillary tube to waste in order to match the optimum uptake rate of the nebulizer (400 $\mu\text{L}/\text{min}$).

The 30 and 50 nm gold nanoparticle CE separation was conducted in 75 μm ID x 80 cm fused capillary with 40 mM SDS and 10 mM CAPS, pH 7.3. The SP-ICPMS dwell time was 10 ms.

Results and Discussion

Assessment of SP-ICPMS accuracy

The validity of the SP-ICPMS theory as described in this report was evaluated by applying it to a series of gold nanoparticles (30, 50, 80, and 200 nm nominal diameter). A suspension of 30 nm gold at $2 \times 10^4 \text{ mL}^{-1}$ was analyzed by SP-ICPMS with a 10 ms dwell time to calculate $q_s \epsilon_n$ from Equation 1, and a 1.0 ng/mL dissolved gold ICPMS standard was analyzed to calculate k in Equation 2. This was then applied to the SP-ICPMS responses (mean $n_{i,p}$ of suspensions of the four nanoparticle standards). The resulting $m_{a,p}$ values were used to calculate the theoretical diameters of corresponding spherical gold nanoparticles. The linear least square fit of the calculated diameters from this procedure against the nominal values (Figure 4) is:

$$d_{\text{calculated}} = 1.00 d_{\text{nominal}} + 0.73; (r^2 = 0.9989).$$

The agreement between the SP-ICPMS calculated diameters and the nominal values demonstrates that the SP-ICPMS theory is valid for gold nanoparticles up to at least 200 nm. At some point, larger particles will not vaporize, atomize and ionize with the same efficiency as dissolved analyte, or their ion plume will not be collected with the same efficiency. At that point, calculated $m_{a,p}$ values will be negatively biased, so quantitative analysis by SP-ICPMS should be evaluated with standards of the largest nanoparticles expected. When nanoparticle standards of well characterized size distribution are not available for a given material, SP-ICPMS should be considered a semi-quantitative technique for measuring particle elemental mass.

There are published studies of the behavior of ion populations in the interface region of the ICPMS mass spectrometer (Macedone, Gammon et al. 2001; Mills, Macedone et al. 2006; Farnsworth, Spencer et al. 2009) and of ion clouds in the plasma produced by single particles (Hobbs and Olesik 1993; Hobbs and Olesik 1997; Gray, Olesik et al. 2009). These studies present the vaporization and ionization, as well as the transmission of ions through the interface, as complex processes influenced by many factors. They might be used to hypothesize that the assumptions made by the SP-ICPMS theory are suspect. However, the results of our investigation demonstrate that the assumptions are valid, at least for gold nanoparticles up to 200 nm diameter.

Precision and selectivity of SP-ICPMS

The precision of SP-ICPMS was assessed by replicate analyses of 50 nm gold nanoparticle suspensions ($4 \times 10^3 \text{ mL}^{-1}$; 5.0 pg/mL). No significant differences in the slopes or positions of the cumulative distribution functions (CDFs) of the detected ion pulses (Figure 5) are detectable. The relative standard deviation of 2.4% for the mean ion counts reflects good precision of the calculated mean particle element mass (Table 4). The relative standard deviation of the pulse count (11%) is consistent with Poisson statistics for a mean of 101, the best precision attainable for the nanoparticle concentration metric.

The selectivity of SP-ICPMS in complex matrices was evaluated by spiking the suspension analyzed in the last two replicates with 60 nm silver nanoparticles at a concentration of $5 \times 10^7 \text{ mL}^{-1}$. Neither the mean particle gold mass nor the gold nanoparticle concentration metric were affected by a greater than 10^4 ratio of silver to gold nanoparticles (Table 4).

Nanoparticle transformation study

There have been several studies of changing size distributions of metal-containing nanoparticles as produced by changes in matrix (Kapoor, Lawless et al. 1994; Peukert, Schwarzer et al. 2005; Shim and Gupta 2007; Baalousha 2009). Increased ionic strength is one factor that often induces greater degree of aggregation, usually attributed to a collapse of the double layer and a decrease of the associated electrostatic repulsion (Domingos, Tufenkji et al. 2009; Gilbert, Ono et al. 2009). SP-ICPMS is a potentially powerful tool for studying nanoparticle transformation processes. Because of the speed of SP-ICPMS analyses, fast transformation processes can be followed. The sensitivity of SP-ICPMS could allow the first studies of transformations at environmentally relevant concentrations.

SP-ICPMS was used to analyze suspension of 60 nm silver over several minutes after the ionic strength was increased by addition of CaCl_2 to a final concentration of 200 mM. The original nanoparticle concentration was similar to those used in most transformation studies to date ($4.5 \times 10^8 \text{ mL}^{-1}$ or 500 ng/mL). The resulting CDFs at 0 (unspiked), 8, and 14 minutes after CaCl_2 addition shift progressively to the right (higher ion counts per pulse) with time (Figure 6). This reflects the expected aggregation to larger particle clusters.

A similar experiment was conducted at a concentration of silver nanoparticles that might be found in a wastewater effluent ($2.2 \times 10^5 \text{ mL}^{-1}$ or 0.25 ng/mL) (Benn and Westerhoff 2008). The transformation was followed over two days, reflecting the slow transformation kinetics expected at low concentration. The CDFs at 0, 1, and 49 hours indicate that at least 85% of the dwell times containing any ion signal produced only 1 or 2 ion counts (Figure 7). This result indicates either dissolved silver or silver nanoparticles of less than about 30 nm diameter. Silver nanoparticles in this experiment appear to dissolve at environmentally relevant concentrations.

The portion of the CDFs with particle mass rank >0.85 shift progressively to the left over time, indicating that the dominant process is a continued dissolution, rather than aggregation. The small number of large nanoparticles (ion counts >200 per particle) does increase over time, indicating slight competing aggregation. This very preliminary study is the first of silver nanoparticle size transformations at environmentally relevant concentrations. It is made possible by the high particle concentration sensitivity of SP-ICPMS.

Screening urban runoff using SP-ICPMS

SP-ICPMS was applied to a small screening-level assessment of metal-containing nanoparticles in a surface water consisting of urban runoff (Las Vegas Wash). Water samples were to be filtered for two reasons. First, it was hoped that a size cutoff of about $0.45\ \mu\text{m}$ could be achieved that would produce data that reflected true nanoparticle content. Second, unfiltered water could contain larger particles ($>5\ \mu\text{m}$) that could potentially clog the nebulizer. The effect of filtration on nanoparticle recovery was studied.

A reagent water suspension of $50\ \text{nm}$ diameter gold nanoparticles ($1 \times 10^4\ \text{mL}^{-1}$) before and after filtration through a $0.45\ \mu\text{m}$ nylon filter (Figure 8a and 8b, respectively) was analyzed by SP-ICPMS. Although the nominal cut-off of the filter is 10 times the diameter of the nanoparticles, the filter retains virtually all the nanoparticles. The CDFs of the unfiltered (Figure 8c) and filtered (Figure 8d) suspensions show that only a few smaller nanoparticles ($< 30\%$ of the original mean particle mass) were recovered in the filtrate. The poor filtrate recovery may indicate adsorption of the nanoparticles on the membrane material.

Recovery studies with reagent water suspensions of $50\ \text{nm}$ gold and $60\ \text{nm}$ silver showed that nearly 100% recovery was obtained in the filtrate using $5.0\ \mu\text{m}$ cut-off nylon filters, so Las Vegas Wash water samples were filtered in the field with these filters. One sample was spiked before filtration with $50\ \text{nm}$ gold and $60\ \text{nm}$ silver nanoparticle suspensions. Even accounting for a 10:1 dilution of silver nanoparticles in the spiked sample, the silver SP-ICPMS analysis of the spiking suspension ($5 \times 10^4\ \text{mL}^{-1}$ – Figure 9a) and the $5.0\text{-}\mu\text{m}$ filtered spiked Las Vegas Wash water sample ($5 \times 10^3\ \text{mL}^{-1}$ – Figure 9b) demonstrate poor recovery. In addition, the CDFs of the spiking suspension (Figure 9c) and the $5.0\text{-}\mu\text{m}$ filtered spiked sample (Figure 9d) show a large bias toward small nanoparticles in the filtered sample. The poor recovery in the real water samples could be due to either adsorption of nanoparticles on larger suspended solids in the spiked sample or a layer of solids on the filter membrane blocking the passage of nanoparticles. An investigation of the mechanism of the poor nanoparticle recovery and of possible approaches to ameliorate the problem is needed. For the preliminary demonstration study reported here, $5.0\text{-}\mu\text{m}$ filtered samples were analyzed to protect the nebulizer, despite the poor recovery. No attempt at correcting results for recovery was made.

Silver-bearing particles are present in the Las Vegas Wash water (Figure 10). The pulse heights indicate a Ag mass equivalent to about 50-nm diameter metallic Ag particles. The particle concentration is approximately $200\ \text{mL}^{-1}$, not correcting for the low recovery. By

contrast, the recovered gold-bearing particle concentration may be on the order of 10 mL^{-1} (Figure 10).

Approximately 400 particles per mL of titanium-bearing particles above an equivalent TiO_2 diameter of about 60 nm are present in Las Vegas Wash water samples (Figure 11). The largest particle is equivalent to about 400 nm TiO_2 .

The SP-ICPMS analysis of Las Vegas Wash water for the lanthanoid elements and yttrium (Figure 12) show the presence of cerium-bearing particles. It is likely that the source is natural, given the presence of the other lanthanoids and yttrium which tend to occur with cerium in minerals.

SP-ICPMS analysis of Las Vegas Wash water at m/z 57, which is the isotope commonly used for iron determination, was conducted at a 10 ms dwell time (Figure 13, upper trace). The continuous signal is largely due to ArOH^+ plasma background. Significant pulses above the background are hard to distinguish. SP-ICPMS analysis with a 3 ms dwell time demonstrates the improved signal-to-noise in SP-ICPMS as dwell time decreases (Figure 13, lower trace). In SP-ICPMS, background is proportional to dwell time, while signal is independent of dwell time, as long as the latter is much longer than the plume pulse transit time, τ_p (Heithmar 2009a). The background signal in Figure 13 is decreased proportionally to the 3/10 dwell time ratio. The background is apparently dominated by flicker noise rather than shot noise, because the background fluctuation appears to decrease nearly as much as the mean background, rather than the square-root relationship produced by shot noise. Significant pulses above the 3 ms background are obvious, indicating iron-bearing particles.

Coupling SP-ICPMS with separation methods

A preliminary investigation of the coupling of SP-ICPMS with HDC separations was conducted. Initial results indicated significant background interference in the SP-ICPMS of gold. SP-ICPMS analysis of SDS eluent from the Agilent reciprocating piston pump (no HDC column) detected numerous background pulses that precluded analysis of HDC chromatograms (Figure 14). It was considered unlikely that the background pulses were due to gold. Tantalum, with a single isotope at m/z 181, is known to form oxide polyatomic ions (m/z 197). The presence of tantalum-containing particles in the SDS eluent was confirmed by the SP-ICPMS analysis at m/z 181 (Figure 14 b). The intensities of the m/z 197 background peaks to the m/z 181 peaks indicate a roughly 1-2% TaO^+ formation relative to the Ta^+ . This is consistent with expected values. Because the tantalum appeared to come from the HPLC pump, the reciprocating piston pump was replaced with a syringe pump. It was hoped that the much slower moving parts of the latter would produce fewer tantalum-bearing particles. The resulting m/z 197 and m/z 181 SP-ICPMS backgrounds revealed only two background peaks greater than 5 ions appear at m/z 197 over a 12 minute period (Figure 15). This level of background is acceptable. Interestingly, the two peaks observed are likely gold, since none of the peaks at m/z 181 are large enough to have produced a pulse of these magnitudes, assuming 2% TiO^+/Ti^+ .

A suspension of 60 nm gold nanoparticles ($50 \text{ pg/mL} - 2.3 \times 10^4 \text{ mL}^{-1}$) was analyzed by HDC coupled to the ICPMS. The m/z 197 chromatogram with 1 s integration time typical for conventional hyphenated analysis includes a poorly defined peak around 760 s, indicating the elution of 60 nm gold (Figure 16a). The small peak at about 830 s is near the elution volume of dissolved gold. The chromatogram of an identical sample at the SP-ICPMS dwell time of 10 ms (Figure 16b) exhibited a group of individual pulses with a mean ion count of about 40-50 at 760 s, consistent with a SP-ICPMS particle gold mass equivalent to 60 nm gold. Thus, the retention time of the HDC peak provides information that the particle diameter is about 60 nm, while the SP-ICPMS signal confirms that the individual particles contain a high fraction of gold. This complementary information would eliminate the possibility in a real analysis that the signal at a 60 nm retention is due to nanoparticles with adsorbed gold or minerals with low gold content.

The HDC-ICPMS chromatogram (conventional 1 s integration windows) of a mixture of 60 nm gold nanoparticles ($50 \text{ pg/mL} - 2.3 \times 10^4 \text{ mL}^{-1}$) and 30 nm gold nanoparticles ($25 \text{ pg/mL} - 9.2 \times 10^4 \text{ mL}^{-1}$) contains peaks around 770 s (50 nm gold) and 785 s (30 nm gold) (Figure 17a). There is no complementary information in the chromatogram to confirm that composition. The HDC-SP-ICPMS chromatogram (10 ms dwell time) includes individual pulses around 770 s producing about 40-50 ions each, while those around 785 s produce about 6-7 ions (Figure 17b). This is in excellent agreement with the ratio predicted by their nominal diameters of about 8:1. One issue with HDC-ICPMS in either the conventional mode or the SP mode is the presence of occasional spurious single particles (see for example the peaks at about 820, 840, and 850 seconds). The cause of these peaks is currently unclear. However, we suspect that they result from contamination from earlier chromatographic runs using larger Au nanoparticles at much higher concentrations ($\mu\text{g/mL}$).

A preliminary experiment coupling CE with SP-ICPMS was conducted with a suspension of 30 nm gold ($4 \times 10^8 \text{ mL}^{-1}$; retention time ca. 13 minutes) and 50 nm gold ($9 \times 10^7 \text{ mL}^{-1}$; retention time ca. 15 minutes). The 30 nm particle concentration in this experiment resulted in a substantial fraction of dwell times with multiple nanoparticles, so the pulse ion-count ratio was less than the expected 5:1 (Figure 18). Nevertheless, the 30 nm and 50 nm particles appear to be nearly completely resolved.

Conclusions and Future Work

The experiments described in this report indicate the promise of SP-ICPMS as a viable metrology tool for metal-containing ENMs. The theory of the technique is valid for gold nanoparticles up to at least 200 nm diameter (83 femtogram mass). Particle element mass and particle concentration measurements are precise and unaffected by large excesses of non-analyte particles.

SP-ICPMS allows the study of nanoparticle size transformation at an environmentally relevant concentration. The particle concentration sensitivity of other methods have previously limited transformation studies to concentrations several orders of magnitude higher. The results presented in this report indicate that, while aggregation is significant at high nanoparticle

concentration ($2.2 \times 10^5 \text{ mL}^{-1}$), dissolution is the dominant transformation process at a more environmentally relevant concentration ($4.5 \times 10^8 \text{ mL}^{-1}$).

SP-ICPMS is a convenient stand-alone method for screening urban runoff water for particles containing substantial mass of a selected analyte element. The method does not respond to high concentrations of particles with low element mass per particle, which complicate analyses by hyphenated methods.

Sample handling artifacts, such as low recoveries of filtered samples, must be addressed to allow reliable screening-level assessments of water containing suspended solids. Alternative methods for removing large particles will be investigated. These methods include filtering with large-area metal sieves and centrifugation.

The coupling of separation methods such as HDC or CE with SP-ICPMS provides more selective analysis than either the separation technique with conventional ICPMS or SP-ICPMS alone. Additional coupled techniques will be investigated. Coupling flow-FFF with SP-ICPMS is particularly promising, given the high resolution of that method compared to HDC. Other emerging techniques such as microfluidic oscillating electric field-FFF may be investigated in collaboration with others.

The main limitation of the SP-ICPMS is its limited nanoparticle concentration dynamic range using commercial ICPMS instruments. This limitation may be largely overcome using a commercial instrument introduced this year that greatly reduces the dead time between individual dwell times, allowing shorter dwell times that increase the upper limit of the dynamic range. Implementation of SP-ICPMS on that instrument is planned soon.

References

- Alvarez, P. J. J., V. Colvin, et al. (2009). "Research Priorities to Advance Eco-Responsible Nanotechnology." ACS Nano 3(7): 1616-1619.
- Baalousha, M. (2009). "Aggregation and disaggregation of iron oxide nanoparticles: Influence of particle concentration, pH and natural organic matter." Science of The Total Environment 407(6): 2093-2101.
- Benn, T. M. and P. Westerhoff (2008). "Nanoparticle Silver Released into Water from Commercially Available Sock Fabrics." Environmental Science & Technology 42: 4133-4139.
- Chaudhry, Q., M. Scotter, et al. (2008). "Applications and implications of nanotechnologies for the food sector." Food Additives & Contaminants: Part A: Chemistry, Analysis, Control, Exposure & Risk Assessment 25(3): 241 - 258.
- Council, National Science and Technology (2010). The National Nanotechnology Initiative - Research and development leading to a revolution in technology and industry.
- Degueldre, C. and P. Y. Favarger (2004). "Thorium colloid analysis by single particle inductively coupled plasma-mass spectrometry." Talanta 62(5): 1051-1054.
- Degueldre, C., P. Y. Favarger, et al. (2004). "Zirconia colloid analysis by single particle inductively coupled plasma-mass spectrometry." Analytica Chimica Acta 518(1-2): 137-142.
- Degueldre, C., P. Y. Favarger, et al. (2006). "Gold colloid analysis by inductively coupled plasma-mass spectrometry in a single particle mode." Analytica Chimica Acta 555(2): 263-268.
- Domingos, R. F., N. Tufenkji, et al. (2009). "Aggregation of Titanium Dioxide Nanoparticles: Role of a Fulvic Acid." Environmental Science & Technology 43(5): 1282-1286.
- Ebenstein, Y., E. Nahum, et al. (2002). "Tapping Mode Atomic Force Microscopy for Nanoparticle Sizing: Tip-Sample Interaction Effects." Nano Letters 2(9): 945-950.
- Farnsworth, P. B., R. L. Spencer, et al. (2009). "A comparison of ion and atom behavior in the first stage of an inductively coupled plasma mass spectrometer vacuum interface: Evidence of the effect of an ambipolar electric field." Spectrochimica Acta Part B: Atomic Spectroscopy 64(9): 905-910.
- Filella, M., J. Zhang, et al. (1997). "Analytical applications of photon correlation spectroscopy for size distribution measurements of natural colloidal suspensions: capabilities and limitations." Colloids and Surfaces A: Physicochemical and Engineering Aspects 120(1-3): 27-46.

Geranio, L., M. Heuberger, et al. (2009). "The Behavior of Silver Nanotextiles during Washing." Environmental Science & Technology 43(21): 8113-8118.

Gilbert, B., R. K. Ono, et al. (2009). "The effects of nanoparticle aggregation processes on aggregate structure and metal uptake." Journal of Colloid and Interface Science 339(2): 285-295.

Gray, P. J., J. W. Olesik, et al. (2009). Particle Size Effects on Vaporization in Laser Ablation Inductively Coupled Plasma Mass Spectrometry. Pittsburgh Conference on Analytical Chemistry and Applied Spectroscopy, Chicago, IL.

Handy, R., F. von der Kammer, et al. (2008). "The ecotoxicology and chemistry of manufactured nanoparticles." Ecotoxicology 17(4): 287-314.

Hassellöv, M. (2009). Detection and Characterization of engineered nanoparticle in the environment using Field-Flow Fractionation coupled to ICP-MS in single nanoparticle detection mode. Goteborg Setac Europe.

Hassellöv, M., B. Lyvén, et al. (1999). "Sedimentation Field-Flow Fractionation Coupled Online to Inductively Coupled Plasma Mass Spectrometry New Possibilities for Studies of Trace Metal Adsorption onto Natural Colloids." Environmental Science & Technology 33(24): 4528-4531.

Hassellöv, M., J. Readman, et al. (2008). "Nanoparticle analysis and characterization methodologies in environmental risk assessment of engineered nanoparticles." Ecotoxicology 17(5): 344-361.

Heithmar, E. M. (2009a). Characterization of metal-containing nanoparticles in water, U.S. Environmental Protection Agency.

Heithmar, E. (2009b). "Characterizing Metal-based Nanoparticles in Surface Water by Single-Particle ICPMS." 237th ACS National Meeting, Salt Lake City, Utah.

Heithmar, E. (2009c). "Single particle ICPMS for characterizing metal-based nanoparticles and monitoring transformation processes in surface water." SETAC Europe Meeting, Gothenburg, Sweden.

Hobbs, S. E. and J. W. Olesik (1993). "The effect of desolvating droplets and vaporizing particles on ionization and excitation in Ar inductively coupled plasmas." Spectrochimica Acta Part B: Atomic Spectroscopy 48(6-7): 817-833.

Hobbs, S. E. and J. W. Olesik (1997). "The influence of incompletely desolvated droplets and vaporizing particles on chemical matrix effects in inductively coupled plasma spectrometry: time-gated optical emission and laser-induced fluorescence measurements." Spectrochimica Acta Part B: Atomic Spectroscopy 52(3): 353-367.

Huff, B. V. and G. L. McIntire (1994). "Determination of the electrophoretic mobility of polystyrene particles by capillary electrophoresis." Journal of Microcolumn Separations 6(6): 591-594.

Kammer, F. v. d., M. Baborowski, et al. (2005). "Field-flow fractionation coupled to multi-angle laser light scattering detectors: Applicability and analytical benefits for the analysis of environmental colloids." Analytica Chimica Acta 552(1-2): 166-174.

Kapoor, S., D. Lawless, et al. (1994). "Reduction and Aggregation of Silver Ions in Aqueous Gelatin Solutions." Langmuir 10(9): 3018-3022.

Kim, T., C.-H. Lee, et al. (2008). "Kinetics of gold nanoparticle aggregation: Experiments and modeling." Journal of Colloid and Interface Science 318(2): 238-243.

Klaine, S. J., P. J. J. Alvarez, et al. (2008). "NANOMATERIALS IN THE ENVIRONMENT: BEHAVIOR, FATE, BIOAVAILABILITY, AND EFFECTS." Environmental Toxicology & Chemistry 27: 1825-1851.

Koirtyoohann, S. R., J. S. Jones, et al. (1980). "Nomenclature system for the low-power argon inductively coupled plasma." Analytical Chemistry 52(12): 1965-1966.

Lai, C.-Y., B. G. Trewyn, et al. (2003). "A Mesoporous Silica Nanosphere-Based Carrier System with Chemically Removable CdS Nanoparticle Caps for Stimuli-Responsive Controlled Release of Neurotransmitters and Drug Molecules." Journal of the American Chemical Society 125(15): 4451-4459.

Lam, J. W. H. and G. Horlick (1990). "A Comparison of Argon and Mixed Gas Plasmas for Inductively Coupled Plasma-mass Spectrometry." Spectrochimica Acta Part B: Atomic Spectroscopy 45.

Leshner, E. K., J. F. Ranville, et al. (2009). "Analysis of pH Dependent Uranium(VI) Sorption to Nanoparticulate Hematite by Flow Field-Flow Fractionation - Inductively Coupled Plasma Mass Spectrometry." Environmental Science & Technology 43(14): 5403-5409.

Lin, W.-C. and M.-C. Yang (2005). "Novel Silver/Poly(vinyl alcohol) Nanocomposites for Surface-Enhanced Raman Scattering-Active Substrates." Macromolecular Rapid Communications 26(24): 1942-1947.

Liu, F.-K., Y.-Y. Lin, et al. (2005). "Highly efficient approach for characterizing nanometer-sized gold particles by capillary electrophoresis." Analytica Chimica Acta 528(2): 249-254.

Liu, F.-K. and G.-T. Wei (2004). "Adding sodium dodecylsulfate to the running electrolyte enhances the separation of gold nanoparticles by capillary electrophoresis." Analytica Chimica Acta 510(1): 77-83.

Macedone, J. H., D. J. Gammon, et al. (2001). "Factors affecting analyte transport through the sampling orifice of an inductively coupled plasma mass spectrometer." Spectrochimica Acta Part B: Atomic Spectroscopy 56(9): 1687-1695.

Magrez, A., S. Kasas, et al. (2006). "Cellular Toxicity of Carbon-Based Nanomaterials." Nano Letters 6(6): 1121-1125.

Michalet, X., F. F. Pinaud, et al. (2005). "Quantum Dots for Live Cells, in Vivo Imaging, and Diagnostics." Science 307(5709): 538-544.

Mills, A. A., J. H. Macedone, et al. (2006). "High resolution imaging of barium ions and atoms near the sampling cone of an inductively coupled plasma mass spectrometer." Spectrochimica Acta Part B: Atomic Spectroscopy 61(9): 1039-1049.

Monserud, J. H., E. K. Leshner, et al. (2009). Real Time Single Particle-inductively Coupled Plasma-mass Spectrometry for Detection and Characterization of Nanoparticles. 237th ACS National Meeting, Salt Lake City, Utah.

Mueller, N. C. and B. Nowack (2008). "Exposure Modeling of Engineered Nanoparticles in the Environment." Environmental Science & Technology 42: 4447-4453.

Nanotechnologies, The Proect on Emerging (2010). "Environment, Health and Safety Research Inventory." from <http://www.nanotechproject.org/inventories/ehs/>.

Nanotechnologies, The Proect on Emerging (2010). "Nanotechnology Consumer Products Inventory." from <http://www.nanotechproject.org/inventories/consumer/>.

Nomizu, T., H. Hayashi, et al. (2002). "Determination of zinc in individual airborne particles by inductively coupled plasma mass spectrometry with digital signal processing." Journal of Analytical Atomic Spectrometry 17(6): 592-595.

Nomizu, T., H. Nakashima, et al. (1992). "Simultaneous Measurement of the Elemental Content and Size of Airborne Particles by Inductively Coupled Plasma Emission Spectrometry Combined with the Laser Light-Scattering Method." Analytical Sciences 8(4): 527-531.

O'Connor, G. and E. H. Evans (1999). Fundamental aspects of ICP-MS. Inductively Coupled Plasma Spectrometry and its Applications. S. J. Hill. Sheffield, Sheffield Academic Press: 119-144.

Peters, T. M., S. Elzey, et al. (2009). "Airborne Monitoring to Distinguish Engineered Nanomaterials from Incidental Particles for Environmental Health and Safety." Journal of Occupational and Environmental Hygiene 6(2): 73 - 81.

- Petersen, S. L. and N. E. Ballou (1992). "Effects of capillary temperature control and electrophoretic heterogeneity on parameters characterizing separations of particles by capillary zone electrophoresis." Analytical Chemistry 64(15): 1676-1681.
- Peukert, W., H.-C. Schwarzer, et al. (2005). "Control of aggregation in production and handling of nanoparticles." Chemical Engineering and Processing 44(2): 245-252.
- Ponder, S. M., J. G. Darab, et al. (2001). "Surface Chemistry and Electrochemistry of Supported Zerovalent Iron Nanoparticles in the Remediation of Aqueous Metal Contaminants." Chemistry of Materials 13(2): 479-486.
- Pyrz, W. D. and D. J. Buttrey (2008). "Particle Size Determination Using TEM: A Discussion of Image Acquisition and Analysis for the Novice Microscopist." Langmuir 24(20): 11350-11360.
- Quang, C., S. L. Petersen, et al. (1996). "Characterization and separation of inorganic fine particles by capillary electrophoresis with an indifferent electrolyte system." Journal of Chromatography A 732(2): 377-384.
- Schulte, P., C. Geraci, et al. (2008). "Occupational Risk Management of Engineered Nanoparticles." Journal of Occupational & Environmental Hygiene 5: 239-249.
- Schurtenberger, P., M. E. Newmen, et al. (1993). "Environmental Particles." J. Buffle, H.P. van Leeuwen (Eds) 2: 37.
- Shim, J.-Y. and V. K. Gupta (2007). "Reversible aggregation of gold nanoparticles induced by pH dependent conformational transitions of a self-assembled polypeptide." Journal of Colloid and Interface Science 316(2): 977-983.
- Stolpe, B., M. Hassellöv, et al. (2005). "High resolution ICPMS as an on-line detector for flow field-flow fractionation; multi-element determination of colloidal size distributions in a natural water sample." Analytica Chimica Acta 535(1-2): 109-121.
- Takagi, A., A. Hirose, et al. (2008). "Induction of mesothelioma in p53+/- mouse by intraperitoneal application of multi-wall carbon nanotube." Journal of Toxicol Science 33: 105-116.
- Tang, Z., L. Wu, et al. (2009). "Size fractionation and characterization of nanocolloidal particles in soils." Environmental Geochemistry and Health 31(1): 1-10.
- Taylor, H. E. (2001). Inductively Coupled Plasma-Mass Spectrometry: Practices and Techniques. San Diego, Academic Press.
- Taylor, H. E., J. R. Garbarino, et al. (1992). "Inductively coupled plasma-mass spectrometry as an element-specific detector for field-flow fractionation particle separation." Analytical Chemistry 64(18): 2036-2041.

Thomas, R. (2004). Practical Guide to ICP-MS. New York, Marcel Dekker, Inc.

Thurman, E. M. and R. L. Malcolm (1981). "Preparative isolation of aquatic humic substances." Environmental Science & Technology 15(4): 463-466.

Tiede, K., A. B. A. Boxall, et al. (2010). "Application of hydrodynamic chromatography-ICP-MS to investigate the fate of silver nanoparticles in activated sludge." Journal of Analytical Atomic Spectrometry 25(7): 1149-1154.

Tiede, K., M. Hassellöv, et al. (2009). "Considerations for environmental fate and ecotoxicity testing to support environmental risk assessments for engineered nanoparticles." Journal of Chromatography A 1216(3): 503-509.

Zhang, L., D. Pornpattananankul, et al. (2010). "Development of Nanoparticles for Antimicrobial Drug Delivery." Current Medicinal Chemistry 17: 585-594.

Tables

Table 1 Engineered nanomaterials uses in consumer products.

Nanomaterial	Number of products	Common uses (with selected examples)
Silver	121	Nutritional supplements; personal care products (tooth brushes, tooth paste); biocide coating on membranes (gloves, masks, condoms); clothing (socks, underwear, baby apparel); toys and pacifiers; dispersed biocide (washing machines)
Titanium dioxide	32	Resin coatings; personal care products (skin cream, hair dryers); nutritional supplements; catalysts (self-cleaning coatings)
Zinc oxide	30	Sun block
Carbon nanotubes	19	Material construction (sporting goods, automobile and aircraft parts)
Gold	15	Nutritional supplements, personal care products (skin cream); catalysts.
Fullerenes	7	Cosmetics
Cerium oxide	1	Fuel additive

Table 2 Common ENM characterization metrics and selected characterization methods.

Characterization metric	Measurement methods
Size distribution - diameter	SEM, TEM, AFM, DLS, SLS, NTA, flow-FFF, sed-FFF, CE, HDC
Size distribution - mass	Sed-FFF
Specific surface area	adsorption isotherm
Surface charge	ζ potential by DLS
Shape	SEM, TEM, AFM, SLS with DLS or FFF

Table 3 Comparison of SP-ICPMS with hyphenated ensemble methods.

SP-ICPMS	Hyphenated ensemble methods
Measures elemental mass of nanoparticles, not nanoparticle size distribution.	Separate nanoparticles into size fractions diameter, and determine total metal concentration associated with each particle size fraction.
Provides concentration of metal-based nanoparticles, and mass of metal in each particle.	Cannot differentiate large concentration of particles containing little analyte from low concentration with high analyte content. Therefore, no information is provided on number or characteristics of metal-based particles.
Fast analysis (e.g., ≤ 60 seconds)	Lengthy analysis (e.g., 20 – 30 minutes)

Table 4. Statistics of replicate SP-ICPMS analyses of 50 nm gold nanoparticles ($4 \times 10^3 \text{ mL}^{-1}$).

Replicate	Mean number of ions per particle	Number of particles
1	25.6	94
2	25	105
3	26.4	87
4 ¹	26.3	101
5 ¹	25.9	115
Grand mean	25.8	101
% RSD	2.2 ²	11

¹ Replicates 4 and 5 were analyzed in presence of 60 nm silver particles at $5 \times 10^7 \text{ mL}^{-1}$.

² Corresponds to < 0.8% RSD in mean particle diameter.

Figure Captions

Figure 1. Number of environmental health and safety (EHS) research projects initiated since 1998.

Figure 2. Time resolved ICPMS signal for dissolved gold (30 pg/mL) at (a) 10 ms dwell time and (b) 2 s dwell time.

Figure 3. Time resolved ICPMS signal for 50 nm gold nanoparticle suspension (30 pg/mL) at (a) 2 s dwell time and (b) 10 ms dwell time.

Figure 4. Correlation of calculated gold nanoparticle diameter from the particle elemental mass determined by SP-ICPMS vs. the nominal diameter reported by the manufacturer.

Figure 5. CDF of five replicate SP-ICPMS analyses of 50 nm gold nanoparticle suspensions at $4 \times 10^3 \text{ mL}^{-1}$. Replicates 4 and 5 also contained 60 nm silver nanoparticles at $5 \times 10^3 \text{ mL}^{-1}$.

Figure 6. Change in CDF of 60 nm silver nanoparticles (500 ng/mL) over time after spiking with 200 mM CaCl_2 .

Figure 7. Change in CDF of 60 nm silver nanoparticles (0.25 ng/mL) over time after spiking with 200 mM CaCl_2 .

Figure 8. SP-ICPMS of 50 nm gold nanoparticles ($1.0 \times 10^4 \text{ mL}^{-1}$) - (a) time-resolved signal of unfiltered suspension, (b) signal of filtrate suspension - 0.45 μm Nylon filter, (c) CDF of unfiltered suspension, (b) CDF of filtrate suspension - 0.45 μm Nylon filter.

Figure 9. SP-ICPMS of 60 nm silver ENMs - (a) time-resolved signal of $5 \times 10^4 \text{ mL}^{-1}$ spiking solution, (b) signal of Las Vegas Wash water spiked to $5 \times 10^3 \text{ mL}^{-1}$ and then passed through 5.0 μm filter, (c) CDF of $5 \times 10^4 \text{ mL}^{-1}$ spiking solution, (d) CDF of spiked and filtered Las Vegas Wash sample.

Figure 10. Time resolved SP-ICPMS signal of silver and gold in 5.0- μm filtered Las Vegas Wash water.

Figure 11. Time resolved SP-ICPMS signal of titanium in 5.0- μm filtered Las Vegas Wash water.

Figure 12. Time resolved SP-ICPMS signal of lanthanoid elements and yttrium in 5.0- μm filtered Las Vegas Wash water.

Figure 13. Time resolved SP-ICPMS signal of m/z 57 in 5.0- μm filtered Las Vegas Wash water at two dwell times.

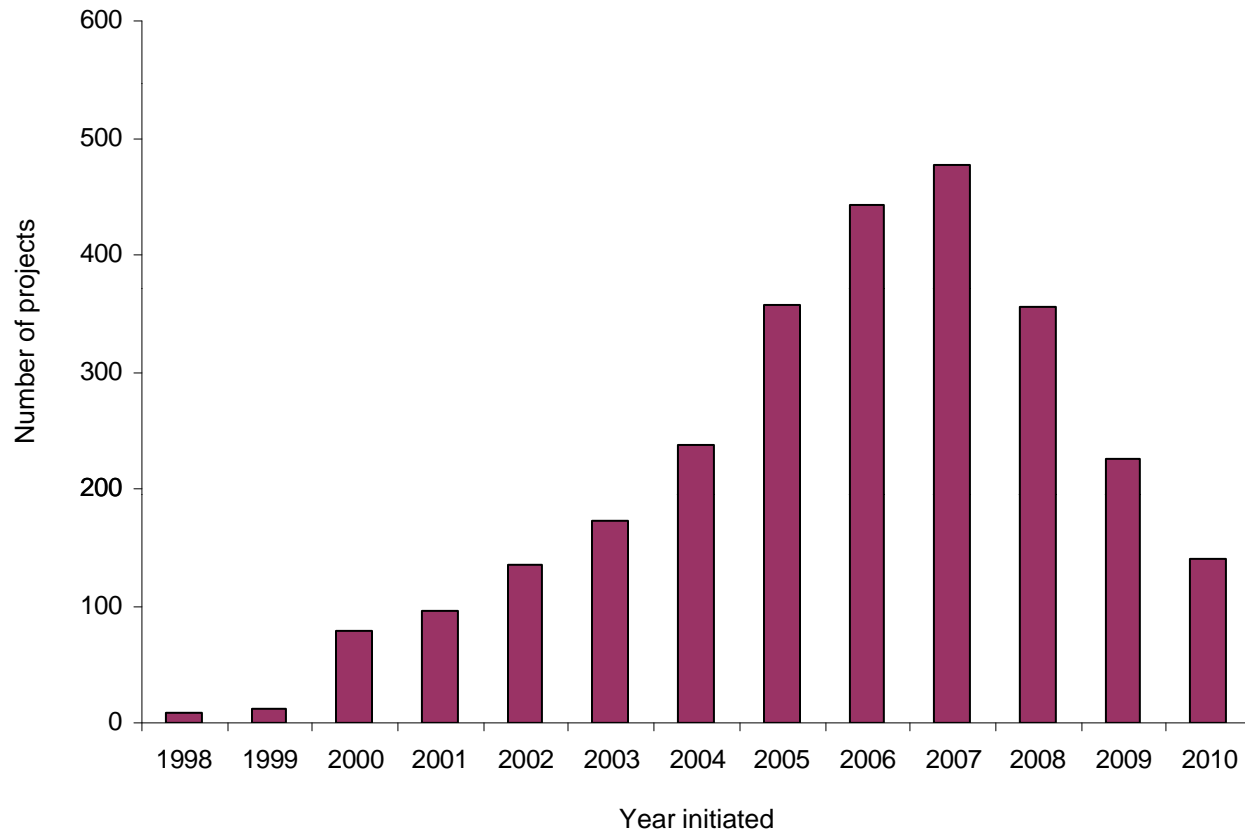
Figure 14. Time resolved SP-ICPMS signal of eluent from liquid chromatograph reciprocating pump – (a) m/z 197 and (b) m/z 181.

Figure 15. Time resolved SP-ICPMS signal of eluent from piston pump – (a) m/z 197 and (b) m/z 181.

Figure 16. HDC-ICPMS chromatograms of 60 nm gold nanoparticles (50 pg/mL) – (a) 1 s dwell time and (b) 10 ms dwell time.

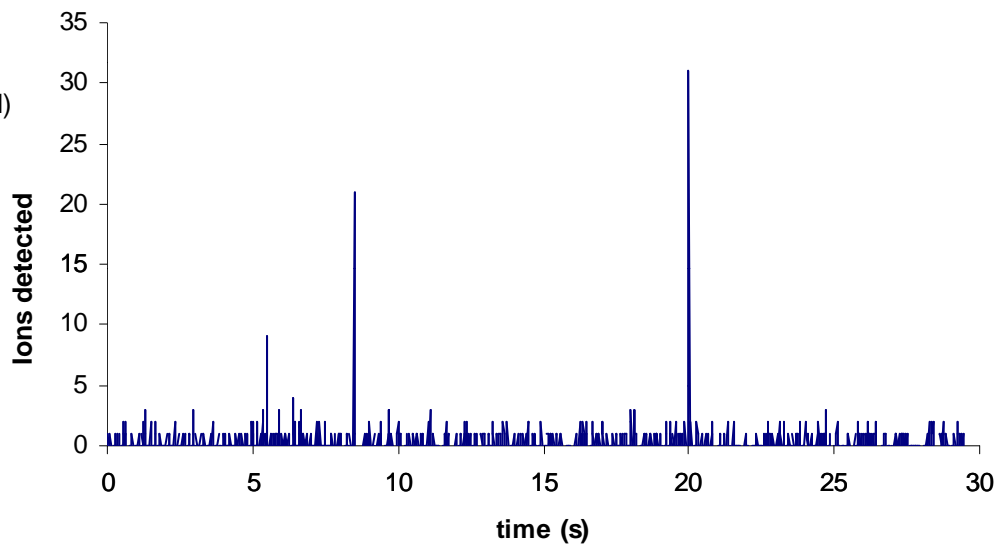
Figure 17. HDC-ICPMS chromatograms of 60 nm gold nanoparticles (50 pg/mL) and 30 nm gold nanoparticles (25 pg/mL) mixture – (a) 1 s dwell time and (b) 10 ms dwell time.

Figure 18. CE-SP-ICPMS electropherogram of 30 nm and 50 nm gold nanoparticles.



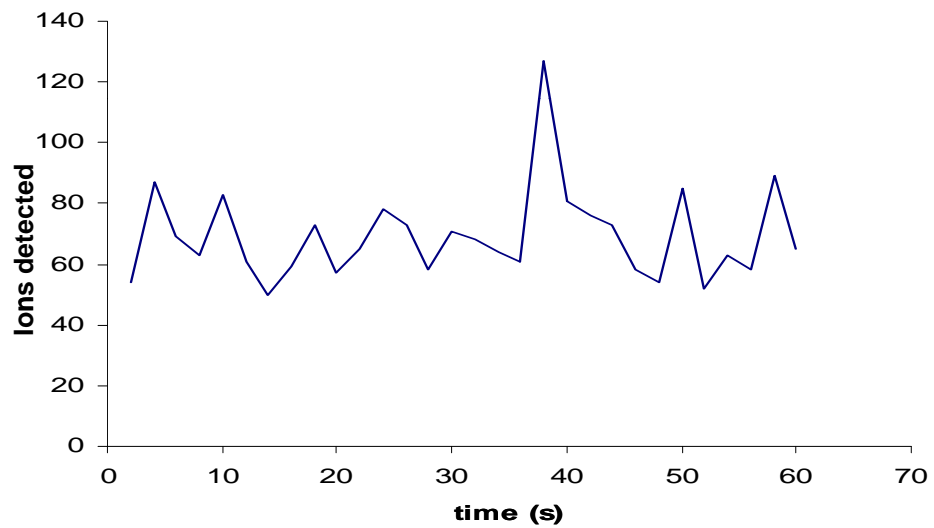
a

ICPMS (dissolved)
10 ms dwell time



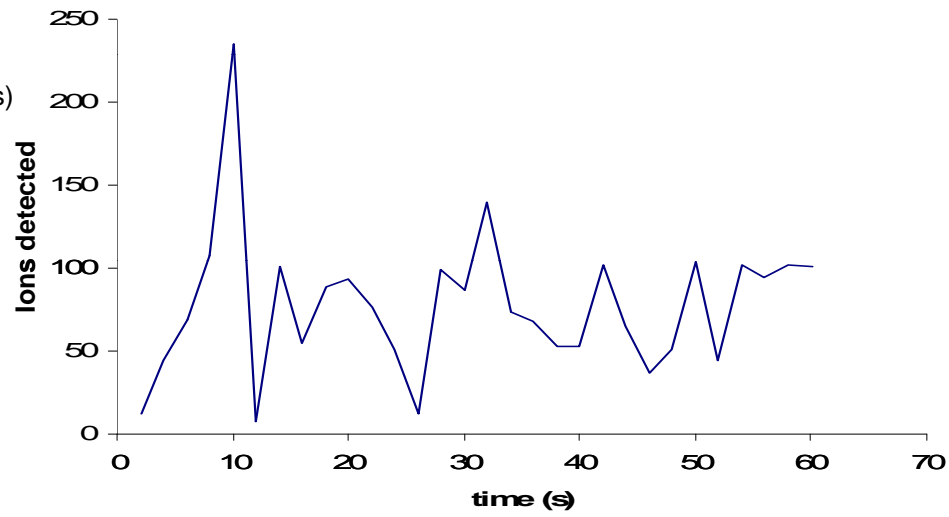
b

ICPMS (dissolved)
2 s dwell time



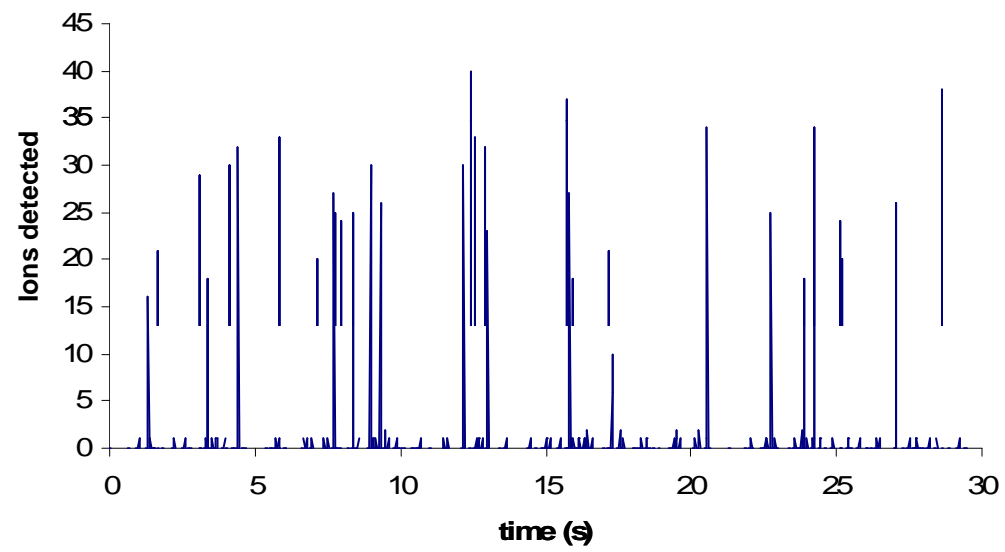
a

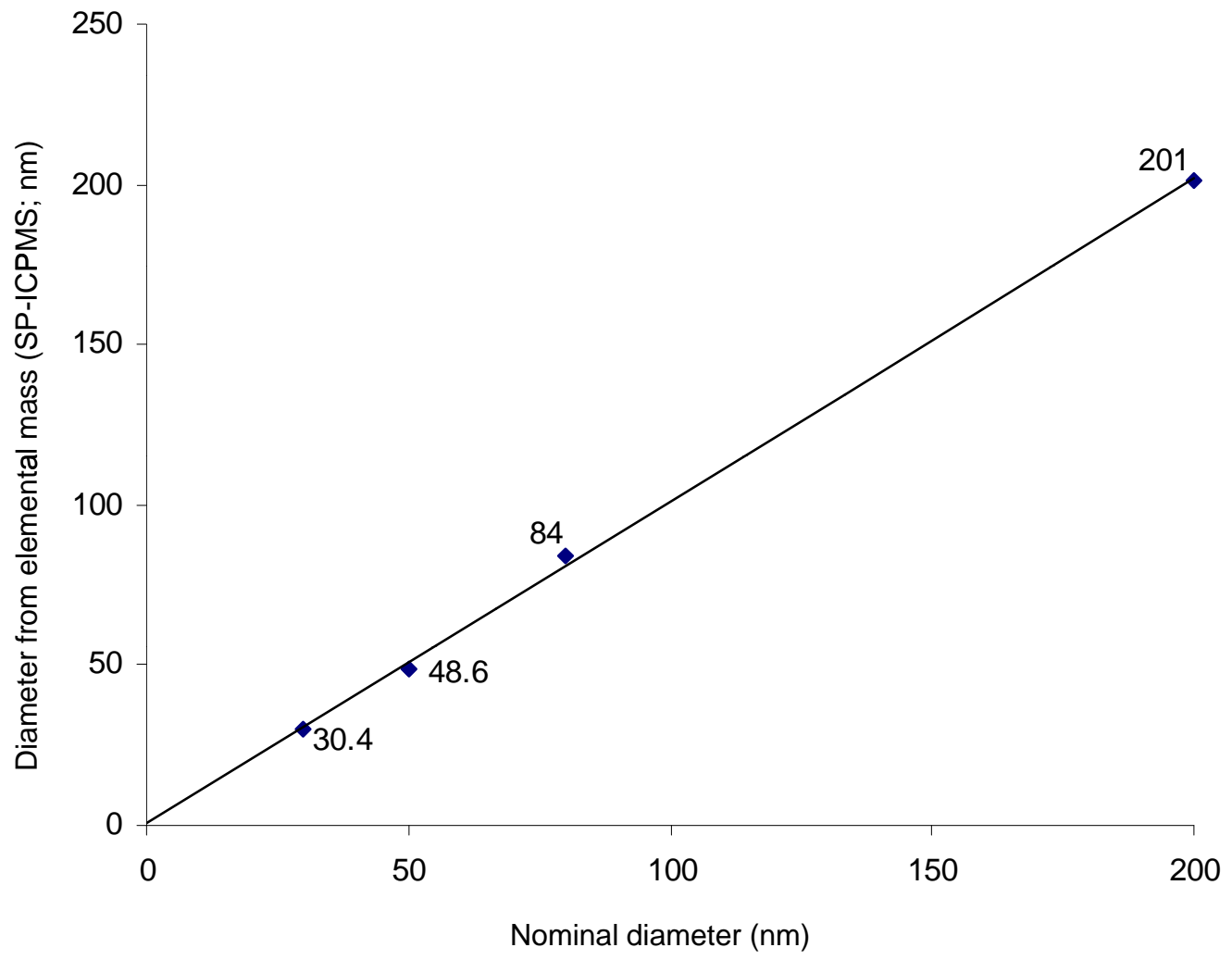
ICPMS (nanoparticles)
2 s dwell time

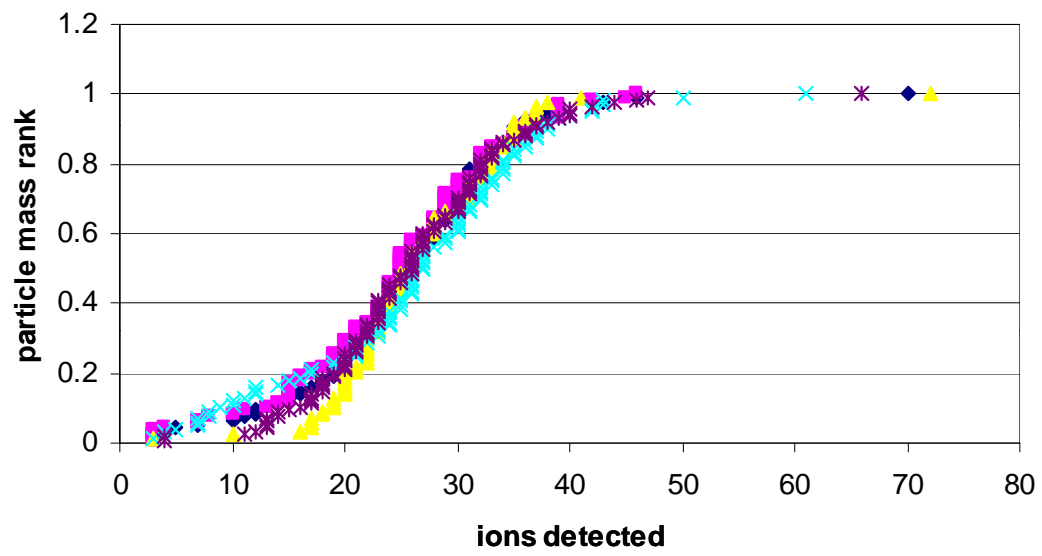


b

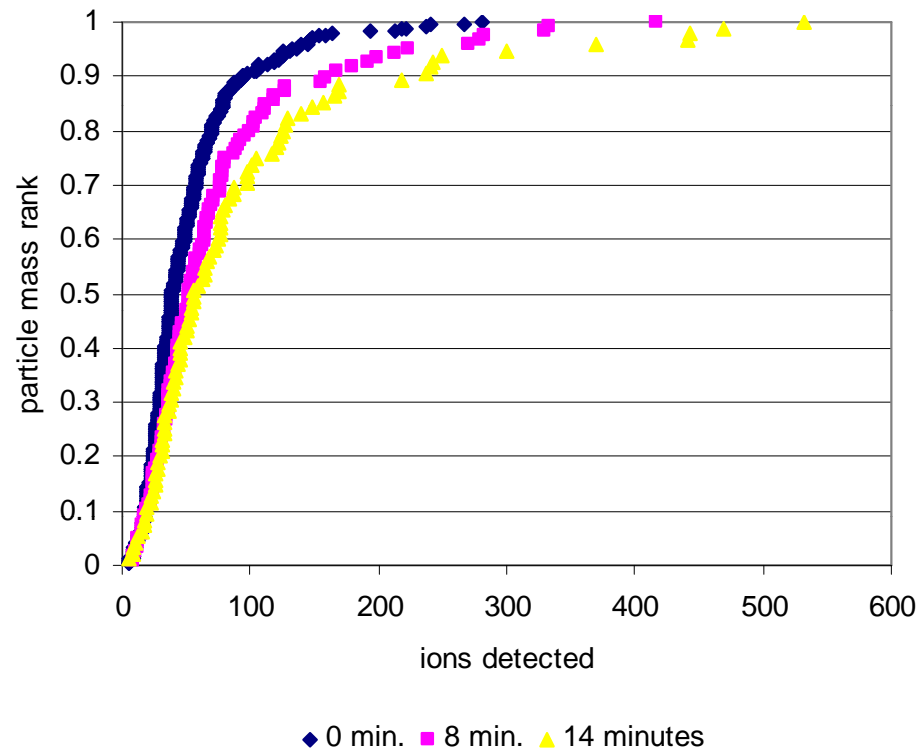
ICPMS (nanoparticles)
10 ms dwell time

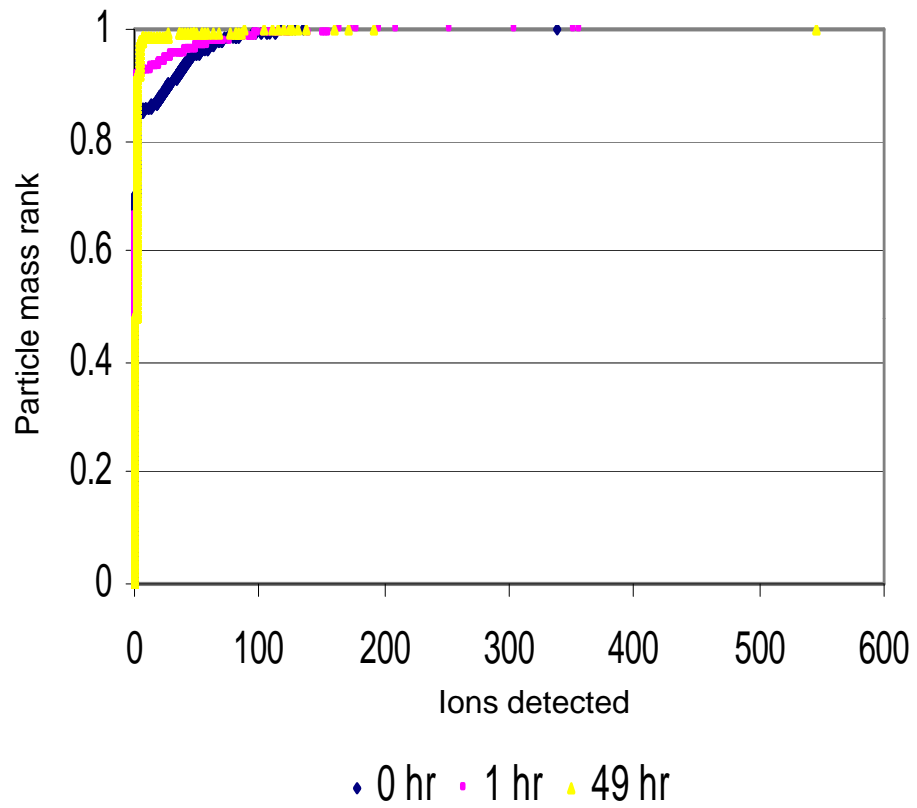


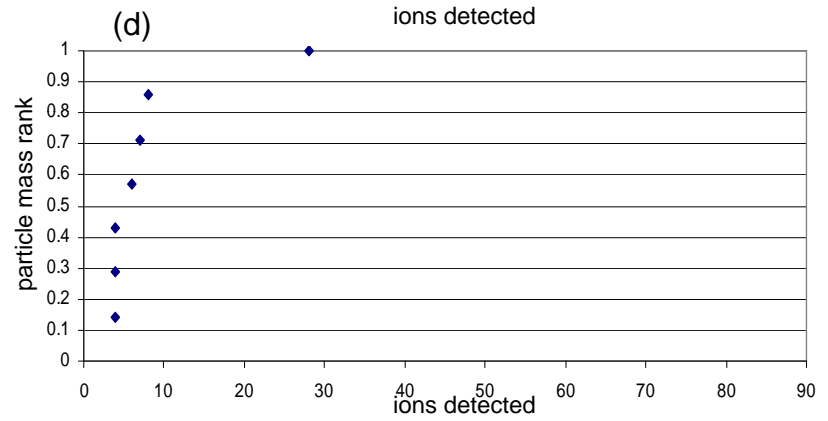
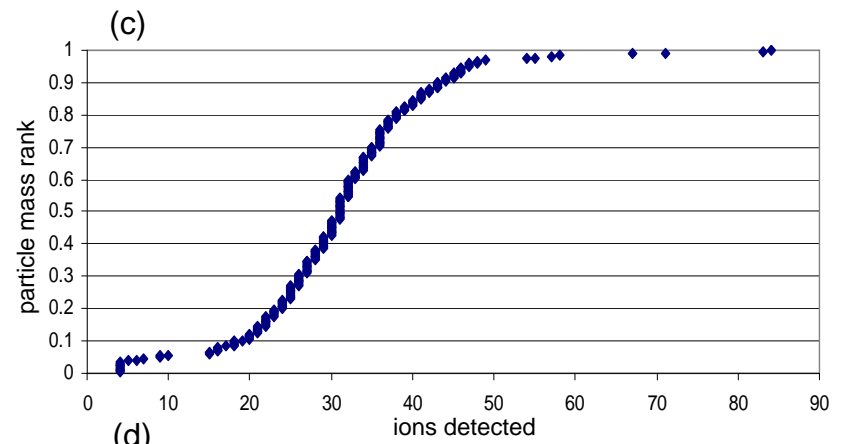
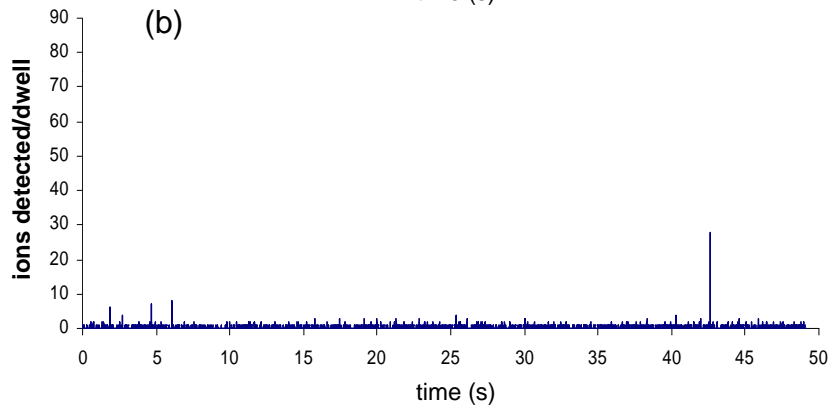
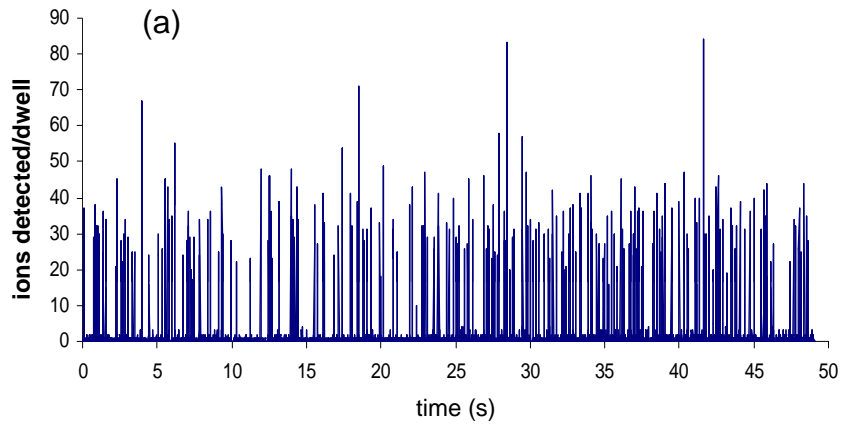


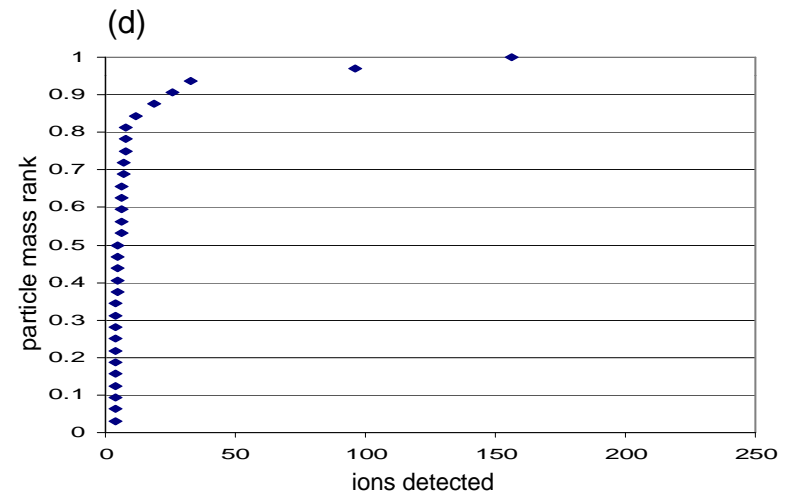
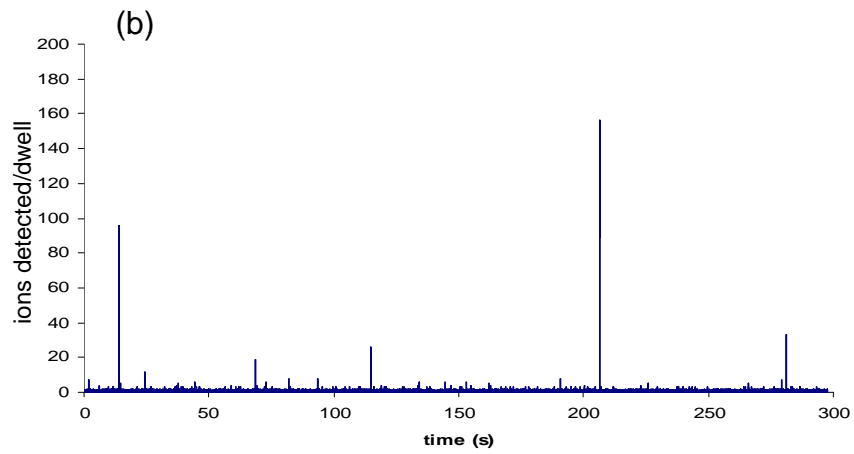
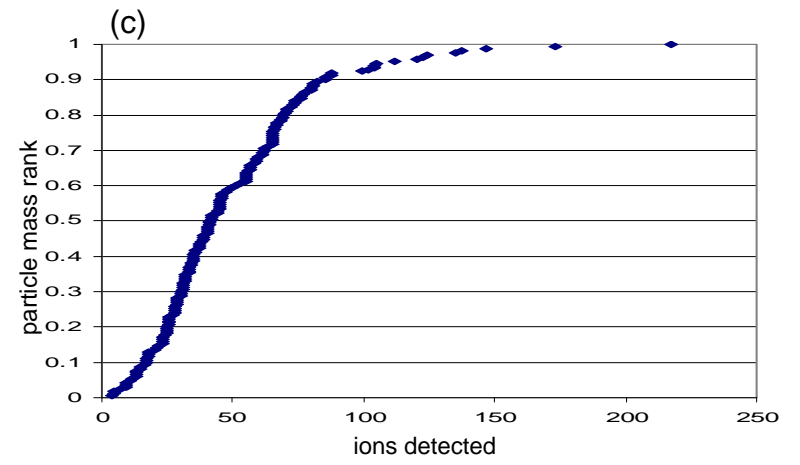
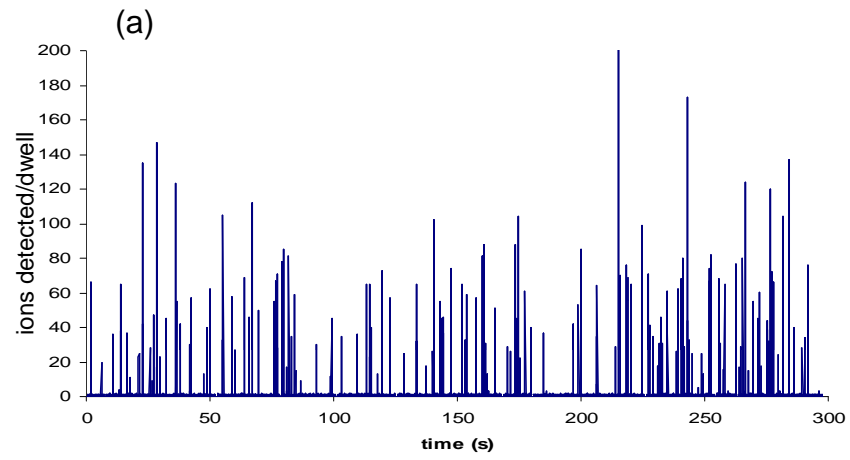


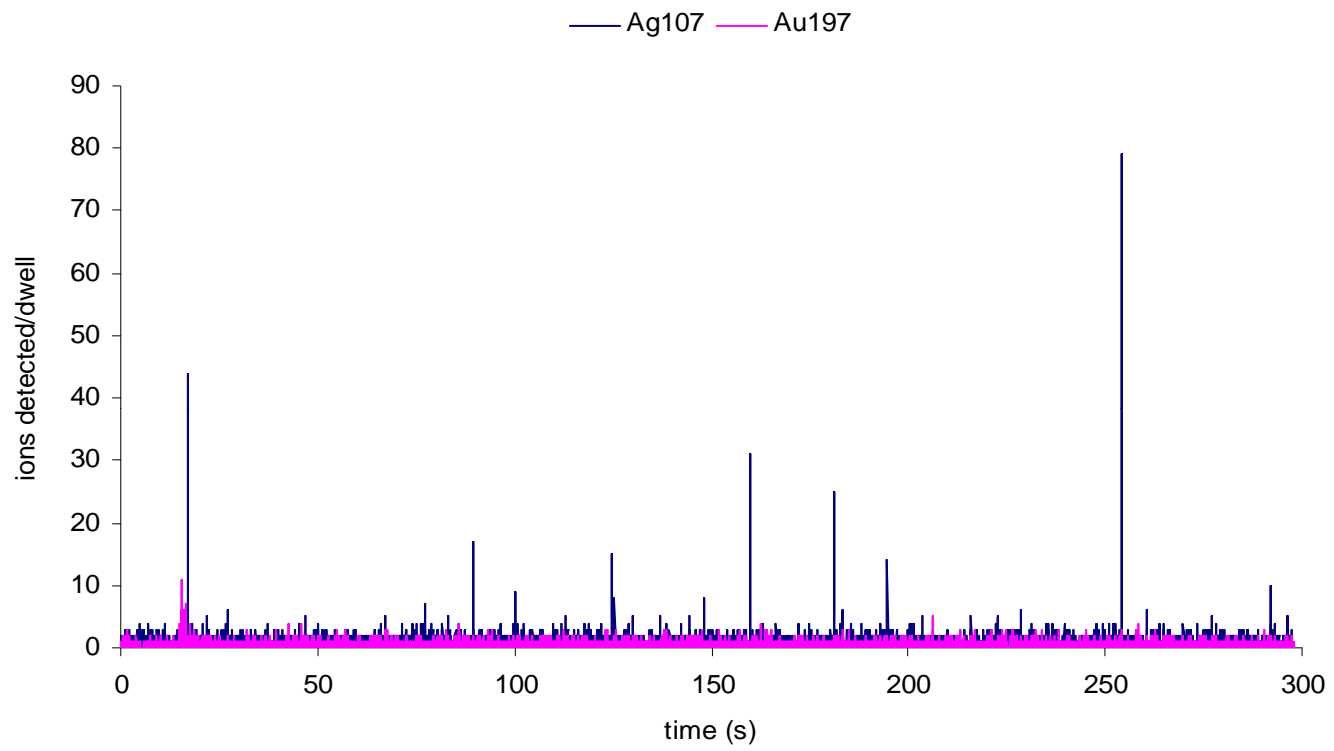
◆ Rep. 1 ■ Rep. 2 ▲ Rep. 3 × Rep. 4 * Rep. 5

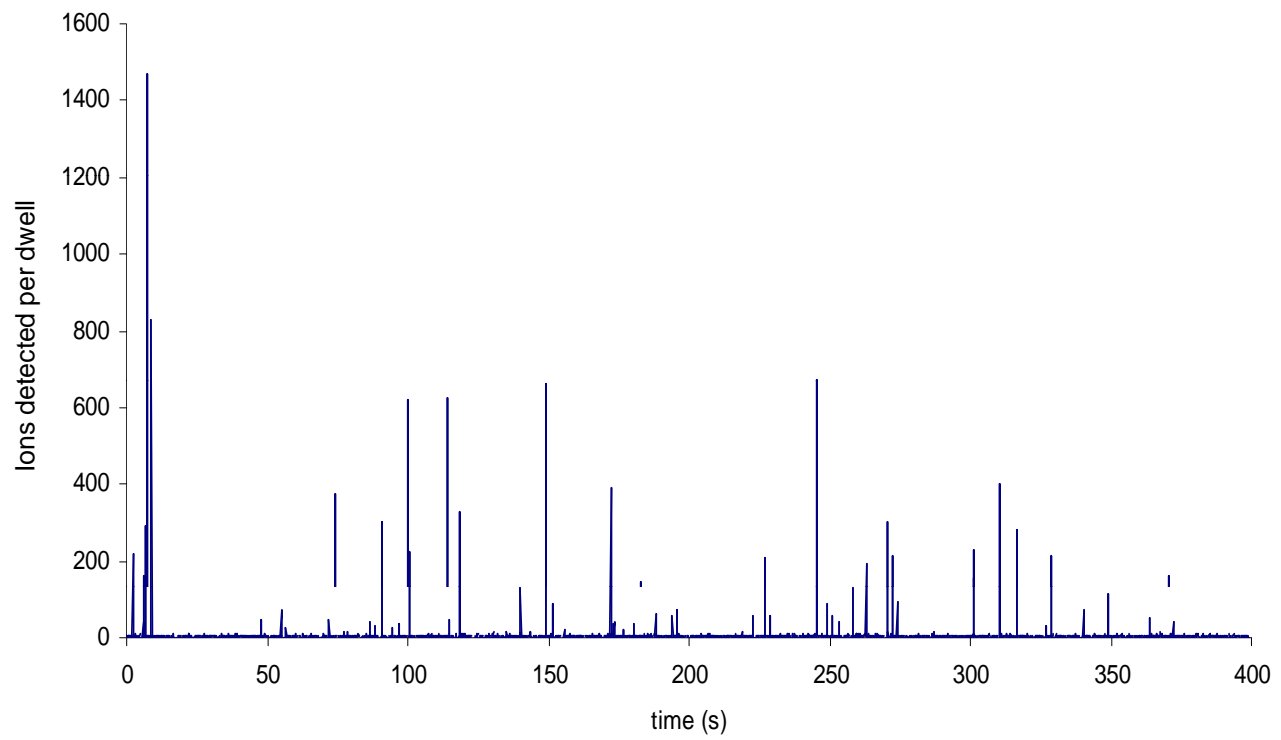


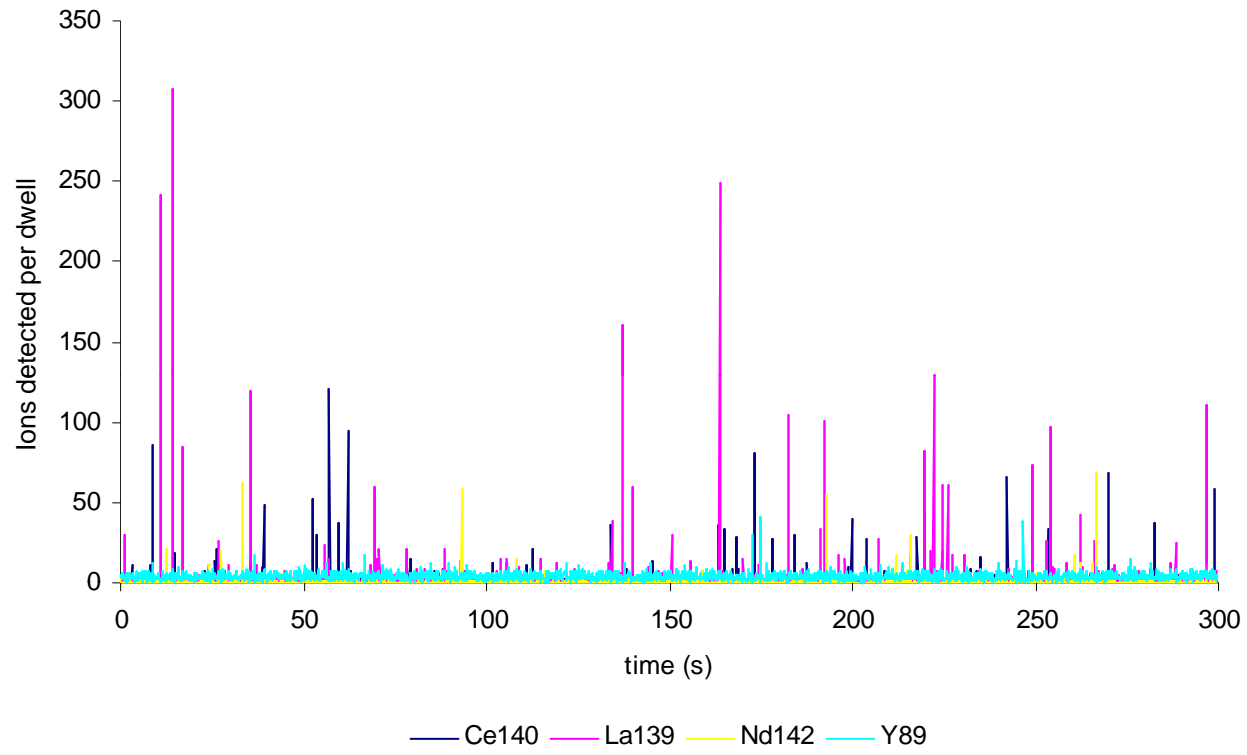


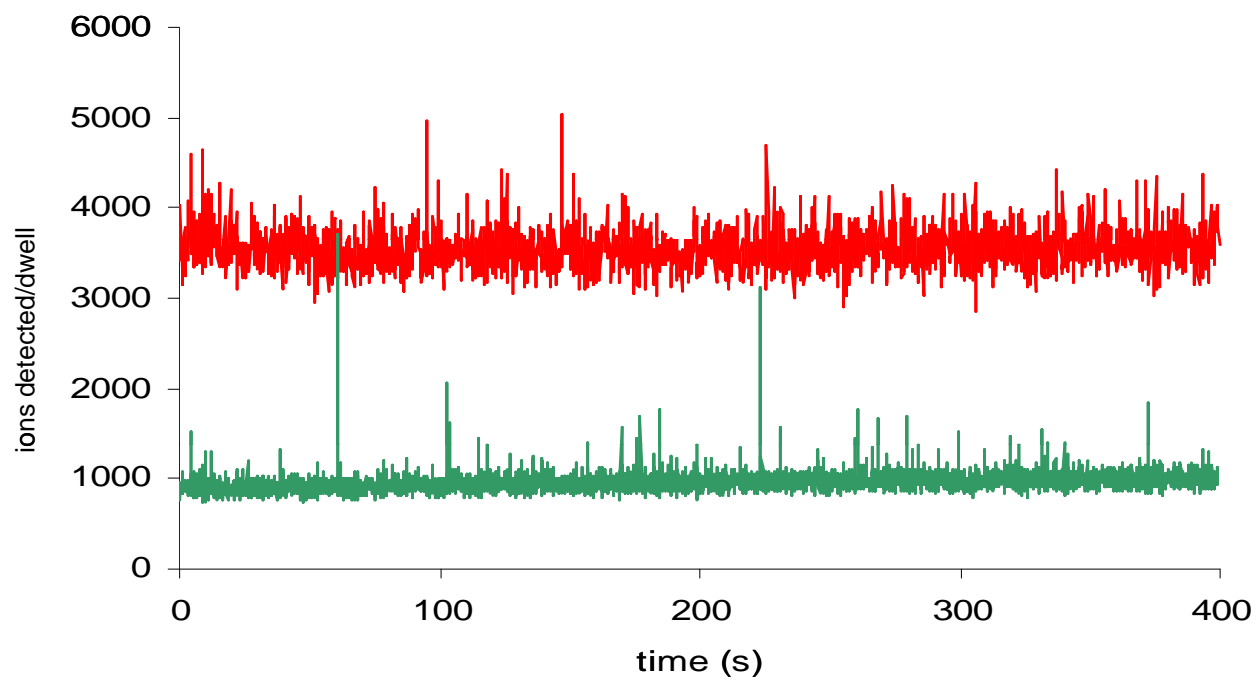








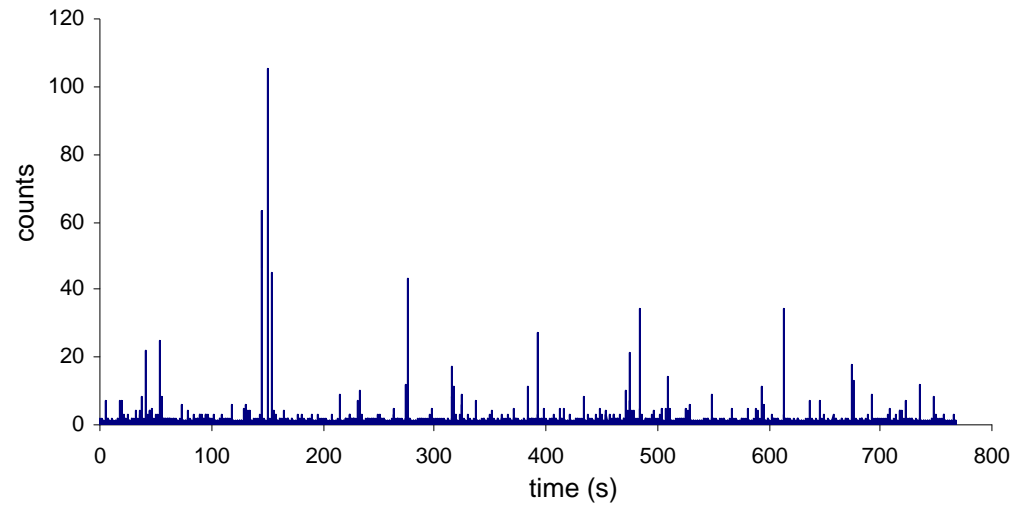




— 10 ms dwell time — 3 ms dwell time

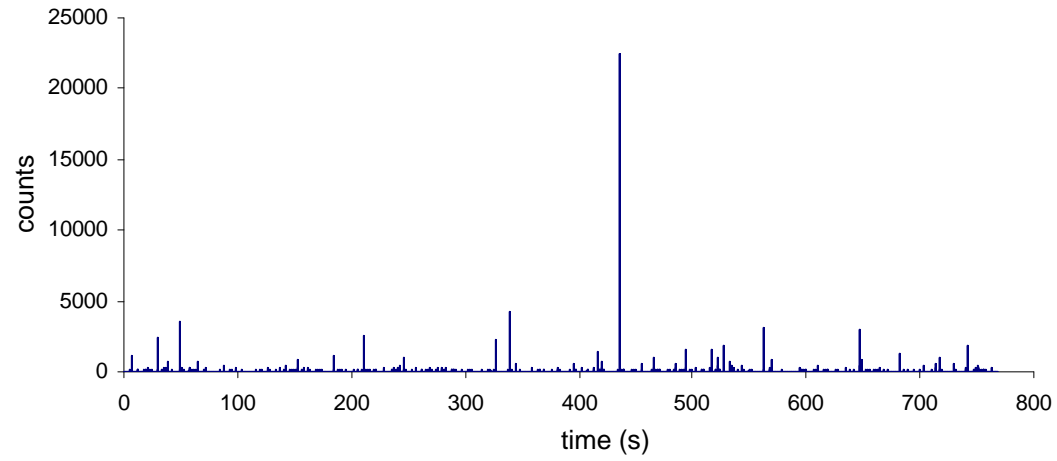
a

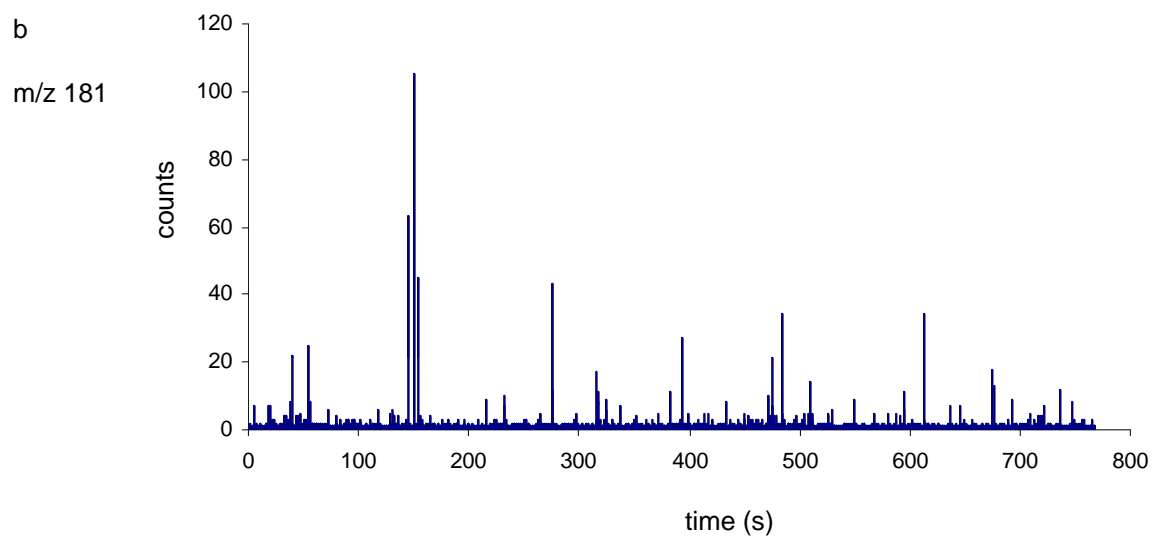
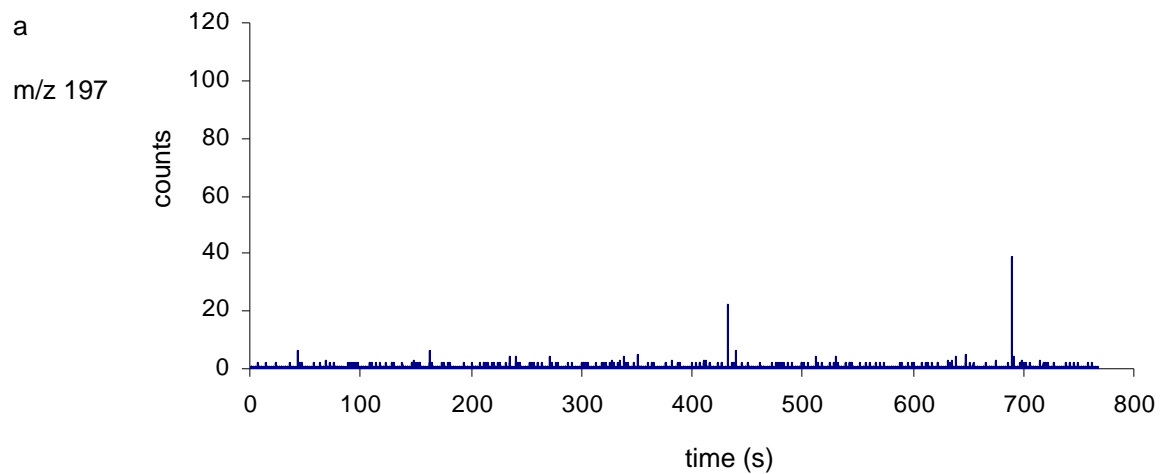
m/z 197

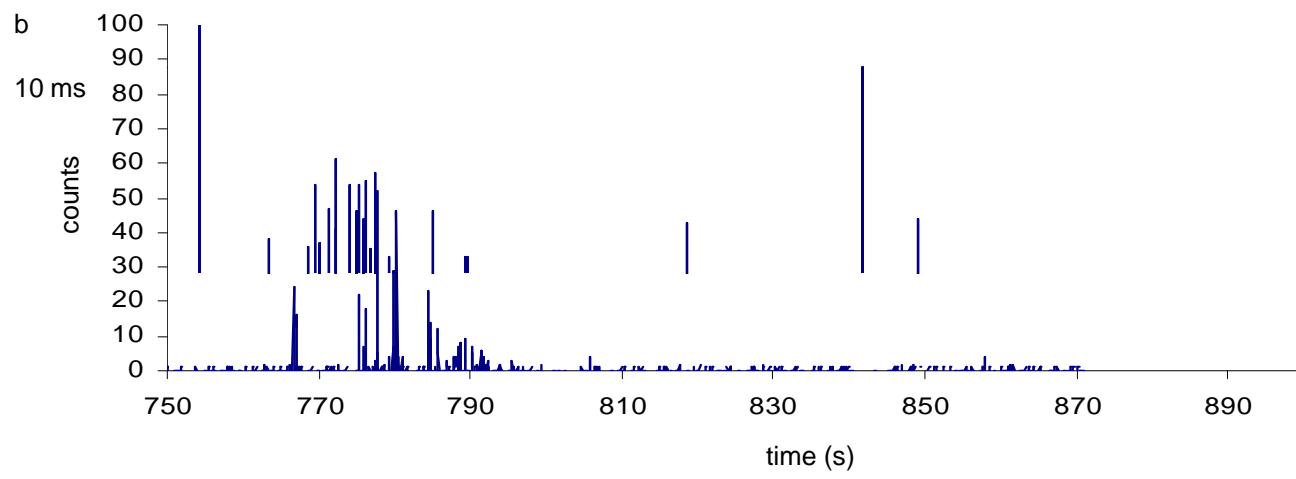
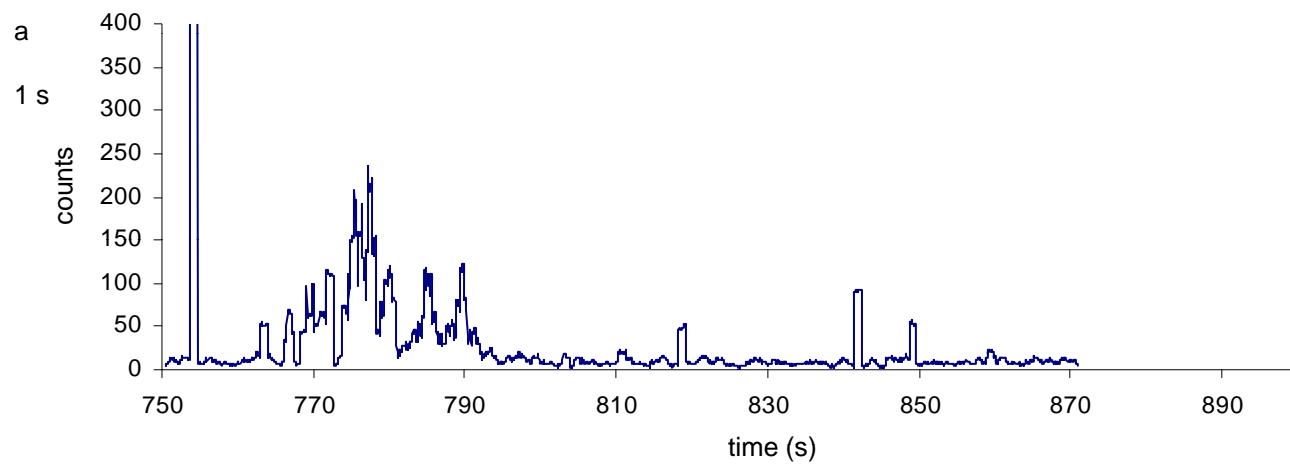


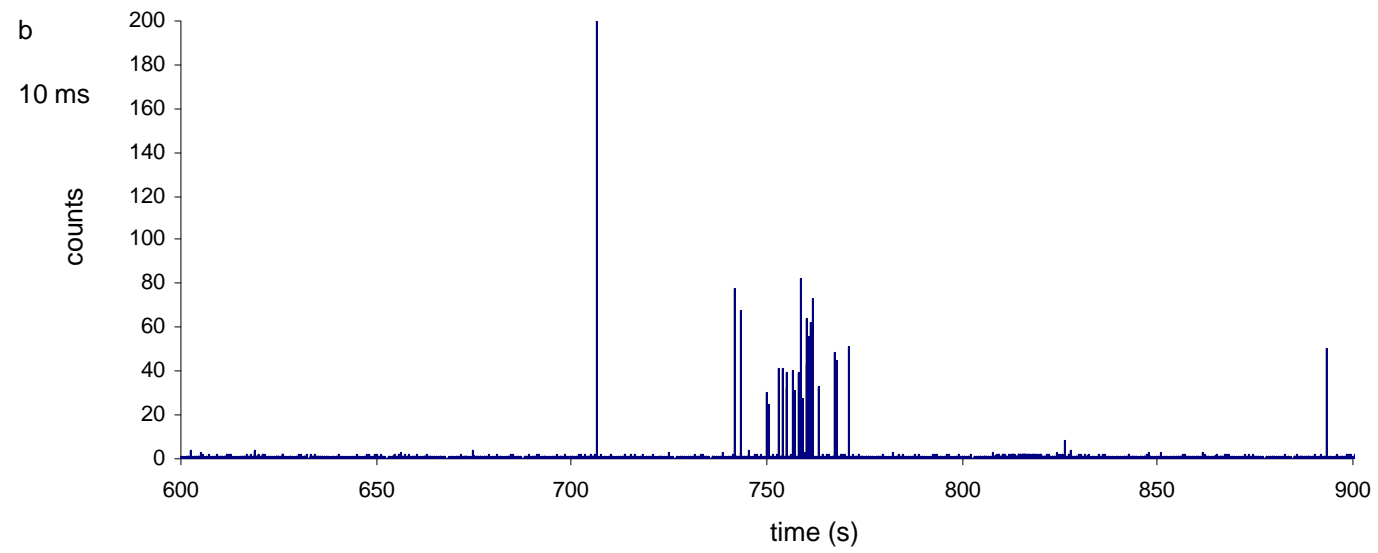
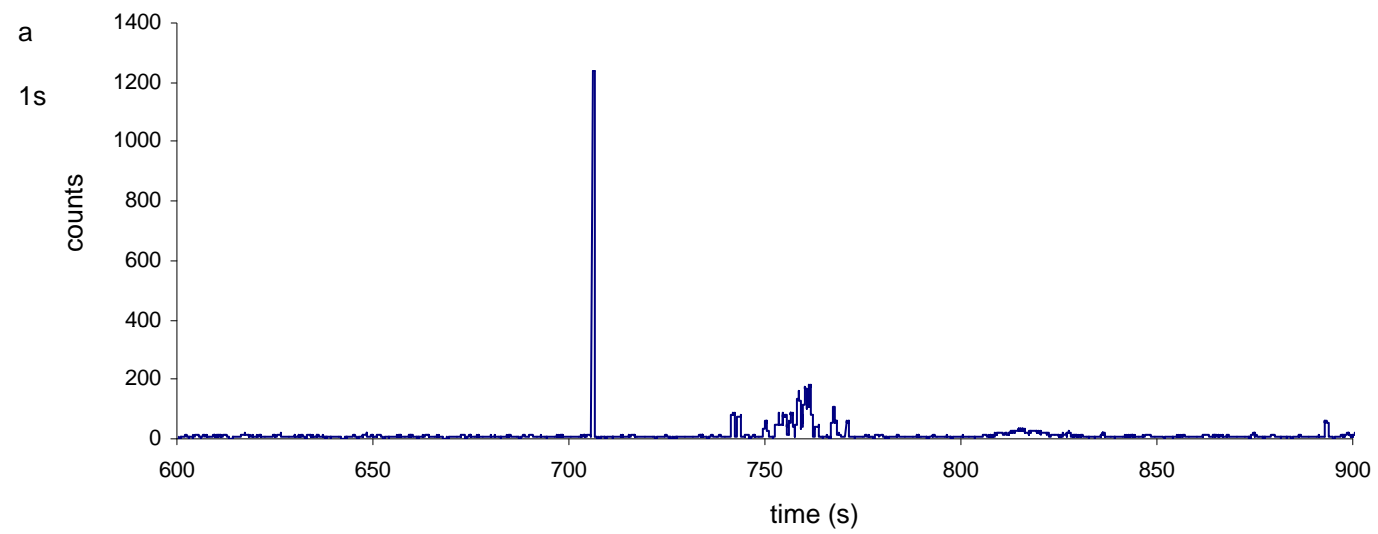
b

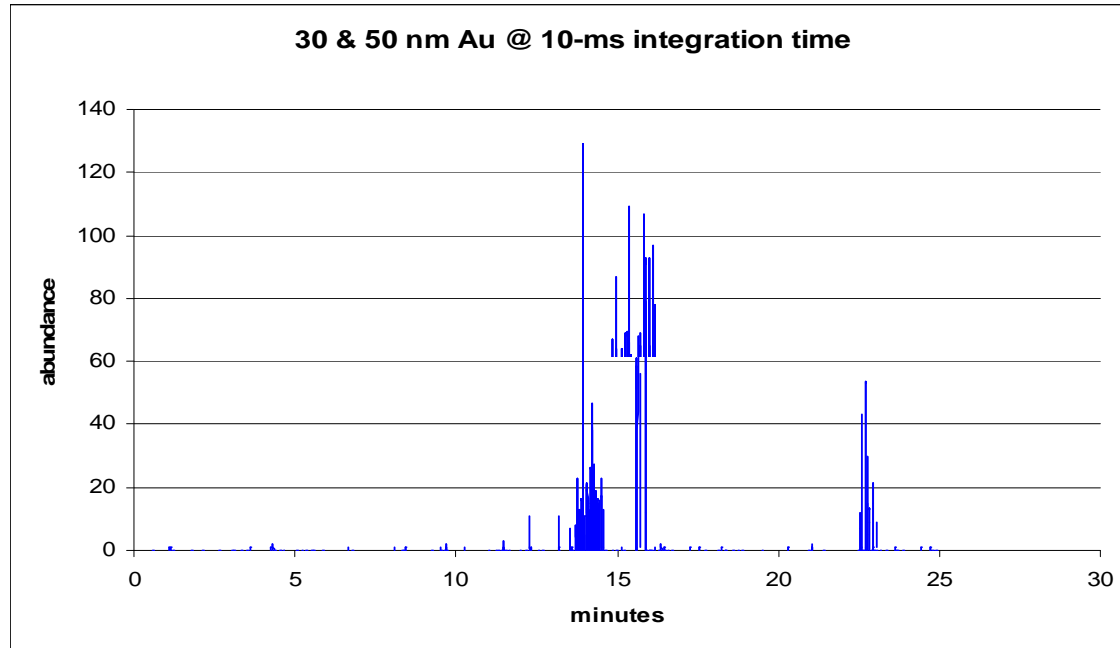
m/z 181













United States
Environmental Protection
Agency

Office of Research
and Development (8101R)
Washington, DC 20460

Official Business
Penalty for Private Use
\$300

EPA/600/R-10/117
October 2010
www.epa.gov

Please make all necessary changes on the below label, detach or copy and return to the address in the upper left hand corner.

If you do not wish to receive these reports CHECK HERE ; detach, or copy this cover, and return to the address in the upper left hand corner.

PRESORTED STANDARD
POSTAGE & FEES PAID
EPA PERMIT No. G-35



Recycled/Recyclable

Printed with vegetable-based ink on paper that contains a minimum of 50% post-consumer fiber content processed chlorine free